University of Alberta

THE EFFECT OF HUMIDITY ON AEROSOL DRUG DELIVERY FROM METERED-DOSE INHALERS

by

Andrew Robert Martin 

A thesis submitted to the Faculty of Graduate Studies and Research in partial fulfillment of the requirements for the degree of **Master of Science**.

Department of Mechanical Engineering

Edmonton, Alberta
Fall 2004

Your file Votre référence
ISBN: 0-612-95816-7
Our file Notre référence
ISBN: 0-612-95816-7

To Mom and Dad, in thanks for years
of support and encouragement.

Acknowledgments

Many thanks go to Dr. Warren Finlay for his continuous guidance and supervision of the work leading to this thesis. In addition, thanks to both Dr. Daniel Kwok and Dr. Carlos Lange for their insightful suggestions and observations along the way. All of my colleagues continue to make the aerosol research lab a wonderful place to come to work each day. Special thanks to Helena Orszanska, whose laboratory expertise has saved me many headaches over the past two years.

Finally, the financial support of the Alberta Ingenuity Fund and the Natural Sciences and Engineering Research Council of Canada is greatly appreciated.

Contents

List of Tables

List of Figures

Chapter 1

An Introduction to Inhaled Pharmaceutical Aerosols and Mechanical Ventilation

1.1 History

The treatment of respiratory disorders through inhalation therapy is certainly not a new phenomenon. Rather, records of our early ancestors are peppered with accounts of the inhalation of vapors for perceived medical benefit. More than 4000 years ago, Hindu physicians advised smoking certain dried spices and leaves as a means of treating throat and chest ailments (1). Ancient Greeks sent those afflicted with pulmonary consumption to the forests of Libya, where they could breath the gases released by pine trees (2). In Egypt, plants were placed on hot bricks so that their medicinal vapors could be inhaled (2).

By the early nineteenth century, the majority of therapies continued to depend on burning of plants or resins in order to release vapors for inhalation. Popular at the time were Potter's asthma cigarettes, which contained shredded stramonium leaves mixed with tobacco (2). Towards the middle part of the century, large glass-bulb devices, capable of atomizing liquids into droplets, began appearing in physicians' offices. These devices, used to clear the upper and lower airways, were the predecessors of modern inhalation systems. It was not the vapor, but rather the *aerosol* (a gasborne suspension of liquid or solid particles) that carried the active, medicinal ingredient.

Not surprisingly, demand for outpatient treatment of asthma led to refinements over the bulky, expensive atomizers used by physicians. In 1938, the hand-bulb

nebulizer was introduced (1). This device consisted of a glass bottle and rubber bulb, the latter squeezed to release an extremely inconsistent mist of droplets. Not surprisingly, the resulting dosage levels were highly variable. Nevertheless, the popularity of such delivery systems spurred inventors towards development of the modern jet nebulizer, as well as new, alternative devices. The introduction of the metered-dose inhaler in 1956 by Riker Laboratories (1) gave patients an effective, highly portable delivery device for the first time.

Today, inhaled aerosols provide optimal treatment of respiratory disorders, including asthma, cystic fibrosis, emphysema, and bronchitis. In addition, researchers are targeting the lung's alveolar region as a gateway to the bloodstream, making possible systemic delivery of vaccinations, treatment of diabetes, and management of pain. Naturally, to meet such diverse applications, a wide variety of delivery systems are now commercially available, with many more in development.

1.2 Delivery Systems

Devices used for the delivery of inhaled pharmaceutical aerosols may be divided into three main categories. Each category has its own advantages and disadvantages; newer technologies should not be considered as direct replacements for their predecessors. The choice of device depends strongly on requirements for portability and dosage, as well as the formulation options of the drug.

1.2.1 Nebulizers

Nebulizers contain drug dissolved, or sometimes suspended, in water. The relative ease of formulating aqueous solutions can be advantageous. In cases where the drug is insoluble in water, a polar organic solvent such as alcohol or propylene glycol may be substituted (3). The most common example of this family of devices is the jet nebulizer, illustrated in Figure 1.1. The nebulizer is supplied with a flow of pressurized air from a compressor or pump. This air is accelerated to high velocity through a nozzle,

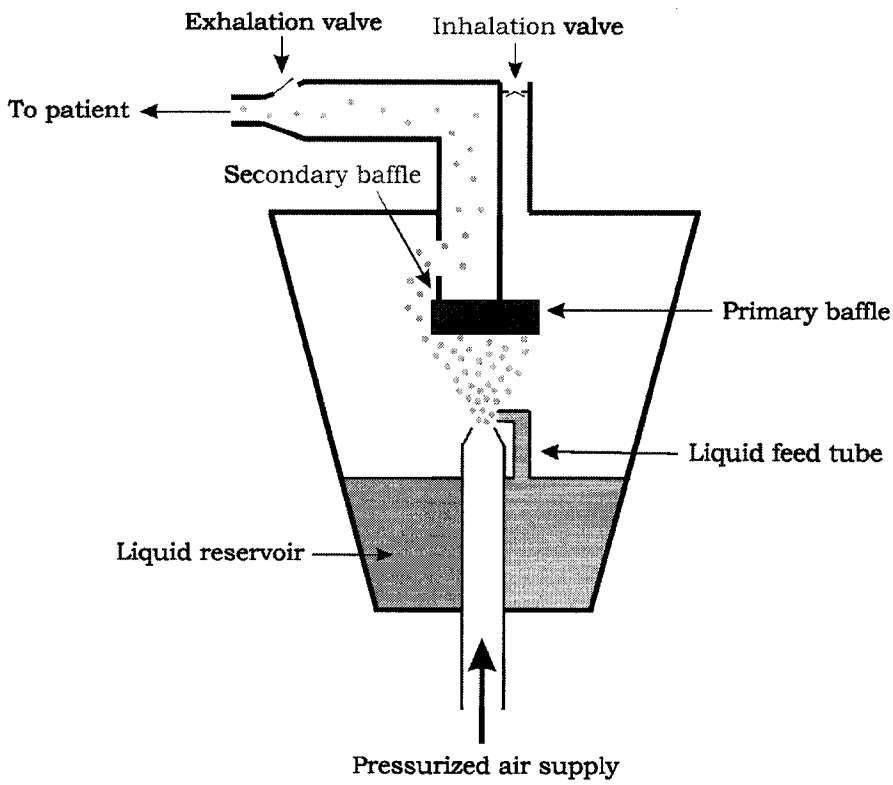

Figure 1.1 Schematic of a typical nebulizer design (adapted from Finlay (4)).

and exits as a jet. The pressure drop associated with the high jet velocity draws liquid up from a reservoir through a liquid feed tube. At the point where liquid meets jet, mechanical forces lead to an initial production of droplets. These droplets are reduced in size through aerodynamic breakup and impaction on a primary baffle. Secondary baffles act as low-pass filters, selectively removing larger droplets from the airflow and returning them to the reservoir. A detailed analysis of droplet production in nebulizers can be found in Finlay (4).

Due to the need of an external supply of air, nebulizers tend not to be portable. Devices that form droplets by ultrasonic vibrations are available, but still require a source of power. In addition, a typical nebulizer operating time might last 15 minutes. As a result, use of nebulizers is generally restricted to the hospital or the home.

1.2.2 Metered-Dose Inhalers

The metered-dose inhaler, abbreviated MDI, is the most commonly used device for delivery of pharmaceutical aerosols. MDIs are small, lightweight, and require no power supply. As a result, they are most widely employed as portable devices for delivery of bronchodilators and corticosteroids in the treatment of asthma and chronic obstructive pulmonary disease.

An MDI formulation consists of a suspension, or solution, of micronized drug particles in a highly volatile, propellant liquid. A co-solvent may be added to enhance drug solubility, or to allow for the addition of a surfactant, which in turn may act as a stabilizer or lubricant. For the propellant to remain in liquid phase, the formulation is contained under pressure inside a valved aluminum canister. The canister is placed inside

a plastic actuator, which includes an exit nozzle and mouthpiece. Prior to actuation, an outlet valve at the base of the canister is closed, while a valve within the canister remains open, allowing a desired dose of formulation to fill a small metering chamber (see Figure 1.2). When the canister is depressed, the metering valve closes and the output valve opens, so that the contents of the chamber flow rapidly through an expansion chamber, then exit the nozzle as liquid droplets at high velocities. The volatile propellant rapidly evaporates, leaving behind an aerosol of residual drug particles for inhalation.

In an effort to reduce deposition of MDI particles in a patient's mouth and throat, add-on devices are often prescribed. Such devices provide more time for propellant to

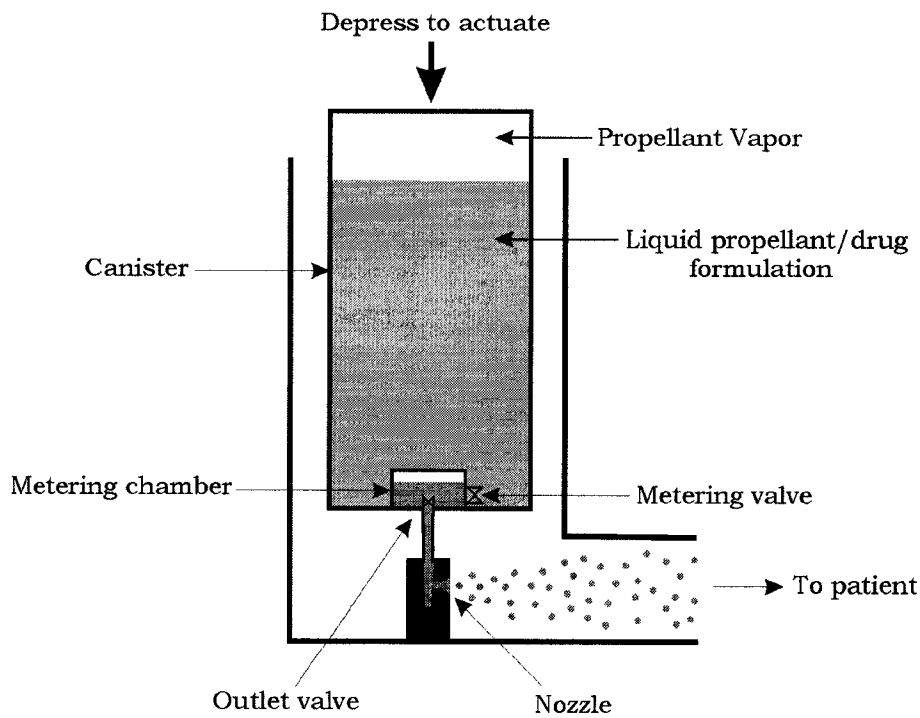

Figure 1.2 Schematic of a typical MDI design (adapted from Finlay (4)).

evaporate, yielding smaller inhaled particle sizes, and a greater distance over which particles decelerate as they are entrained into inspiratory airflow, reducing particle momentum. In addition, add-on devices aid in coordination between MDI actuation and inhalation, a technique many patients, especially children, have difficulty with. Devices which simply increase the distance between the MDI mouthpiece and the patient are generally termed 'spacers', while those which allow the aerosol to settle until the patient inhales one or more times through a valve are referred to as 'holding chambers' (4).

Prior to the 1990s, all MDIs relied on chlorofluorocarbon (CFC) propellants. However, in compliance with the 1989 Montreal Protocol, CFCs are being phased out of use due to their potential for depletion of the ozone layer. After much investigation, hydrofluoroalkanes (HFAs) have emerged as the viable substitute for CFC propellants in MDIs. The high level of research associated with the changeover has helped fuel interest in inhaled drug delivery. However, HFAs themselves have been cited as greenhouse gases in the 1997 Kyoto Protocol. Apprehension over future regulatory pressures (5, 6), in combination with the challenges of designing propellant-based drug formulations, has led industry to focus much of its development on alternative, non-propellant devices, most notably dry powder and new, "soft mist" inhalers. It has therefore been predicted that MDI usage will decline over the next decade, with or without regulatory measures (5, 6).

1.2.3 Dry-Powder Inhalers

Although the dry-powder inhaler (DPI) was first introduced 30 years ago, it has only recently gained popularity as an alternative to the MDI. Currently, DPIs lead the charge of new, innovative delivery devices to the market. They are as portable as an MDI, and often require no power supply. As the name suggests, DPIs do not contain any solvent liquid, but rather present the desired dose of drug in powder form.

In general, the dose of drug delivered from a DPI must be entrained in a patient's inspiratory airflow though aerodynamic lift and drag forces. Normally, large manufactured drug particles must be milled or spray-dried down to respirable sizes, on the order of a few microns in diameter. Unfortunately, dry particles will adhere to any surface, including neighboring particles and device walls, due to short-range, electrostatic, intermolecular attractions (van der Waals forces). At respirable sizes, the aerodynamic forces associated with typical inhalation flow rates cannot overcome particle adhesion (4). To circumvent this problem, larger carrier particles, often lactose or glucose, are added to the formulation. The drug particles adhere to the surface of the carrier, resulting in an agglomerate particle that is much easier to handle. Alternatively, the small drug particles may be tumbled together to form a larger sphere, eliminating the need for a carrier. Whichever method is used, the adhesions that hold the agglomerate particle together must be small enough that they are overcome by aerodynamic loading upon inhalation. With this condition met, the drug particles will separate from the agglomerate, and return to respirable sizes.

Unlike the MDI, it is the patient's inhalation that initially entrains the powder and activates the DPI (although devices that employ an external source of energy for powder

dispersion, so-called 'active' DPIs, are in development). As a result, the difficulty in coordinating the inhalation breath with device actuation that frustrates many MDI users is not of concern when operating a DPI. However, variation in inhalation strength and flow pattern can significantly affect powder entrainment and deaggregation. This can lead to a high variability in the amount of drug successfully delivered. In addition, dry-powder formulations often contain a hydrophilic component, making them sensitive to humidity. Although exposure to humidity in storage can be prevented by a protective cap or foil packaging, powder entrainment into humid airflow can lead to both hygroscopic particle growth and reduced deaggregation of agglomerates, hindering delivery of the drug (7).

The design of DPIs varies greatly from device to device. Descriptions of a number of commercially available powder inhalers can be found in either Dunbar *et al.* (8) or Borgström *et al.* (9).

1.3 Mechanical Ventilation

Mechanical ventilation is required for patients suffering from acute or chronic respiratory distress who cannot supply their bodies with sufficient oxygen through spontaneous breathing. The goal of the ventilator circuit is to reproduce the body's normal breathing pattern. Various modes of mechanical ventilation may be required depending on the condition of the patient, as described by Gammon et al. (10). However, Esteban et al. found in 2000 that of 1,638 patients receiving mechanical inhalation in 412 different intensive care units in North America, South America, Spain, and Portugal, 99% received ventilation through either an endotracheal tube or a tracheostomy (11). For these patients, supplied air bypasses the mouth, throat, and upper trachea, where spontaneously

inhaled air is normally conditioned to body temperature and humidity (37° C and saturated). If the water vapor content of air supplied through an endotrachael tube or tracheostomy is less than that for saturation at body temperature, moisture will be absorbed from the airways, compromising the mucociliary transport system, and thereby increasing bacterial colonization which can lead to ventilator-associated pneumonia (12). Therefore, it is necessary that supplied air be heated and humidified prior to reaching the patient.

Bronchodilator drugs are part of the standard therapy for mechanically ventilated patients (13). These drugs significantly decrease airway resistance in patients with chronic obstructive lung disease (COPD) or asthma, as well as in patients with acute lung injury (13, 14). As with ambulatory patients, the preferred method of delivery of bronchodilators during mechanical ventilation is through the inhalation route. Systemic (intravenous) administration provides no advantage in drug efficacy, and increases the likelihood of side effects (14, 15). By administering the therapeutic agent directly to the respiratory tract through inhalation, systemic side effects are limited.

Traditionally, nebulizers have been employed for the delivery of bronchodilators to mechanically ventilated patients. However, over the past ten years, MDIs have become equally commonplace. When used in combination with an inline spacer or holding chamber (Figure 1.3), and with a proper technique of administration, MDIs have been shown to be at least as effective as nebulizers in the delivery of bronchodilators to ventilated patients (14, 16, 17). Advantages associated with the use of MDIs include increased reliability of dosing, lower risk of contamination, and reduced cost (13).

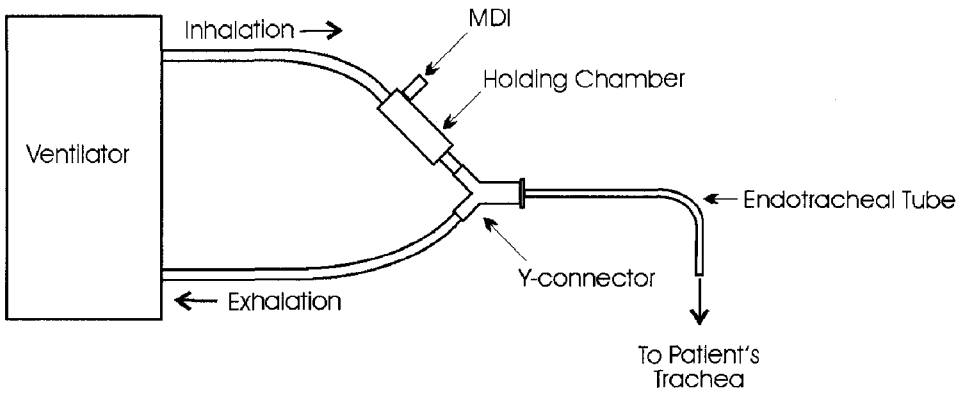

Figure 1.3 Schematic of ventilator circuit with in-line holding chamber for MDI delivery.

Unfortunately, delivery of therapeutic aerosols to the lung is reduced dramatically for both MDIs and nebulizers in the confined, humid environment of the ventilator circuit (17). For delivery of bronchodilators from MDIs, lung deposition has been observed to decrease by up to 50% when normal ventilator conditions (35 to 37° C and >95% relative humidity [RH]) are compared to dry, ambient conditions (25 to 27° C and ≤10% RH) with *in vitro* adult models (14, 17, 18), while equivalent or even higher reductions have been reported for pediatric models (19, 20, 21). Fink et al. have previously demonstrated that aerosol delivery in such *in vitro* models accurately reflects *in vivo* delivery (22).

These reductions in lung deposition have been attributed to a decreased rate of evaporation of propellant from MDI particles (14, 18, 19). Retarded propellant evaporation would lead to larger aerosol sizes in the add-on device (spacer or holding chamber) and subsequent tubing, thereby increasing the probability of inertial impaction in the ventilator circuit prior to the aerosol reaching the patient. Alternatively, several previous authors have proposed that MDI particle sizes increase after complete

evaporation of the propellant, due to hygroscopic or condensative growth of residual drug particles (17, 20, 21, 22). In such a case, the general effect on aerosol deposition would remain the same, in that the probability of impaction in the ventilator circuit would increase. To date, the mechanism by which lung deposition from MDIs is reduced during mechanical ventilation, whether by retarded propellant evaporation, growth of drug particles, or some other phenomenon, has not been established. Such is the focus of the present work.

1.4 Summary of Thesis

The goal of this project was to determine the primary mechanism by which delivery of drug to the lung via MDI is reduced in the warm, humid airflow supplied during mechanical ventilation. With such an understanding, possible approaches for circumventing these losses can be evaluated.

Chapter 2 introduces the terminology and aspects of aerosol mechanics necessary for analysis of MDI drug delivery.

Chapter 3 describes the experimental methods through which the behavior of MDI aerosols in the confined, humid environments typical of ventilator circuits was explored.

Chapter 4 presents the results obtained from these experiments.

Chapter 5 discusses the experimental data, interpreting the results through consideration of the aerosol mechanics introduced in chapter 2.

Chapter 6 provides a concise summary of the thesis.

Chapter 2

A Brief Background in Aerosol Mechanics

2.1 Introduction

The study of inhaled aerosols spans multiple disciplines, broadly including physics, chemistry, pharmacy, medicine, and physiology. The scope of the present chapter is only to introduce some basic aspects of aerosol mechanics relevant to the thesis. Much more detailed reviews of the field of aerosol science, including applications to respiratory deposition, have been provided by Baron and Willeke (23) and by Hinds (24). In addition, Finlay (4) presents an excellent summary of aerosol mechanics as related to the delivery of inhaled pharmaceuticals. The present work has benefited greatly from readings of these three texts.

2.2 Particle Size Distributions

Particle size is a key indicator of where in the respiratory tract an inhaled aerosol will deposit. The vast majority of inhaled aerosols are polydisperse, meaning that they contain particles of a wide range of sizes. Such distributions of size are best characterized by statistical means. This is frequently done under the assumption that particles are spherical, so that size can be specified by a particle's diameter. For inhaled pharmaceutical aerosols, the convention is to treat all particles as spherical particles. In general, such an assumption is reasonable, as liquid aerosol droplets *will* be spherical due to surface tensions, while solid particles are usually compact, so that their motion through the air is not much different from that of a sphere of equivalent volume.

In order to express experimental particle size data statistically, it is necessary to find a suitable distribution function. For most single-source aerosols, the log-normal distribution provides a reasonable fit to experimental data points (24). The log-normal frequency distribution is expressed as

$$f(x) = \frac{1}{x\sqrt{2\pi}\ln\sigma_g}\exp\left[\frac{-(\ln x - \ln x_g)^2}{2(\ln\sigma_g)^2}\right] \tag{2.1}$$

where x — particle diameter;
x_g — count median particle diameter;
σ_g — geometric standard deviation (GSD).

The frequency distribution is defined so that $f(x)dx$ gives the fraction of aerosol particles having diameter between x and $x + dx$. For a log-normal distribution, 68% of the particles have a diameter between x_g/σ_g and $x_g\sigma_g$.

One advantage to using log-normal distributions to characterize particle size is that for spherical particles, a log-normal frequency distribution will give rise to a log-normal volume distribution and (provided all particles have the same density) a log-normal mass distribution, each with the same GSD as the frequency distribution (4). The means and medians of these distributions can be readily calculated from the count median diameter using the Hatch-Chaote conversion equations (23, 24). For example

$$\text{MMD} = x_g \exp\left[3(\ln\sigma_g)^2\right] \tag{2.2}$$

where MMD — mass median diameter.

In the field of inhaled pharmaceutical aerosols, it is most common to express particle size distributions as normalized log-normal mass distributions according to

$$m_{normalized}(x) = \frac{1}{x\sqrt{2\pi}\ln\sigma_g}\exp\left[\frac{-(\ln x - \ln \mathrm{MMD})^2}{2(\ln\sigma_g)^2}\right] \tag{2.3}$$

Here, $m_{\mathrm{normalized}}(x)\mathrm{d}x$ gives the fraction of the total aerosol mass contained in particles having diameter between x and $x + \mathrm{d}x$. Such a distribution is completely characterized by its MMD and GSD.

In many cases, size distributions are provided in terms of the particles' *aerodynamic* diameters, given by

$$x_{aero} = \sqrt{\frac{\rho_{particle}}{\rho_{water}}}x \tag{2.4}$$

where x_{aero} — particle aerodynamic diameter;
x — particle geometric diameter;
ρ_{particle} — density of particle;
ρ_{water} — density of water.

For irregular particles, aerodynamic diameter standardizes shape to that of a sphere, and density to that of water (Figure 2.1). Under the assumptions of a small particle Reynolds number (Stokes flow) and particle diameter much larger than the mean free path of air (continuum assumption)[1], and provided that gravity and fluid drag are the only external forces on a spherical particle, aerodynamic diameter is the only particle

[1] In general, inhaled pharmaceutical aerosols have particle diameters on the order of a few microns and are entrained in a patient's respiratory airflow, so that these two assumptions are valid.

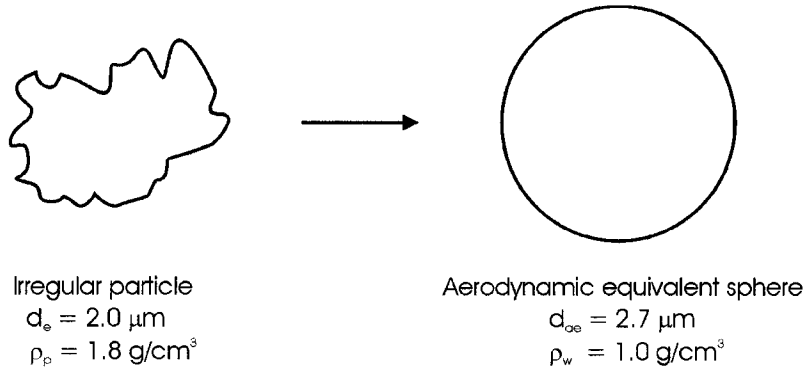

Figure 2.1 An irregular particle with density of 1.8 g/cm^3 and volume equivalent to that of a sphere with diameter of 2.0μm is converted to its aerodynamic equivalent sphere.

property that affects its trajectory (4). This being so, many aerosol sizing instruments rely on particle trajectories to characterize the aerodynamic size distribution of sampled aerosols. Therefore, the normalized mass distribution given by equation 2.3 is frequently expressed in terms of aerodynamic particle diameters, in which case MMD is replaced by MMAD, the mass median *aerodynamic* diameter. The majority of inhaled pharmaceutical aerosols have particle densities close to that of water, so that there is only a small difference between MMD and MMAD. The normalized log-normal mass distribution of a typical inhaled aerosol is shown in Figure 2.2.

2.3 Respiratory Deposition

Aerosol deposition in the respiratory tract is the primary concern in development and evaluation of inhaled pharmaceutical aerosols. In the majority of circumstances, the goal

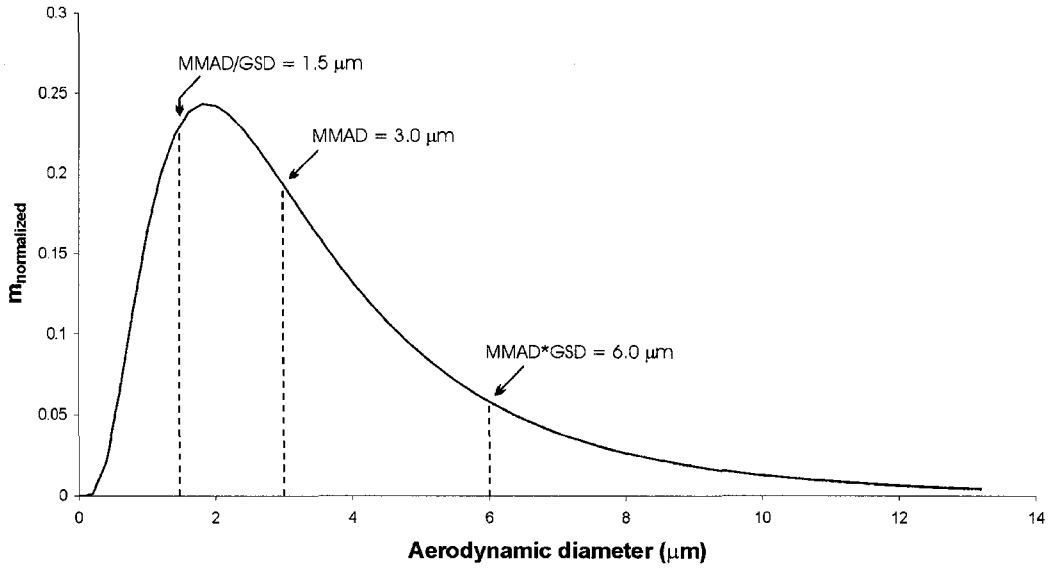

Figure 2.2 Normalized log-normal mass distribution with MMAD = 3.0 μm and GSD = 2.0. 68% of the total aerosol mass is contained in particle sizes between MMAD/GSD and MMAD*GSD.

is to bypass the natural filtering of the mouth and throat and deliver aerosolized drug to the central and/or peripheral regions of the lung. Unfortunately, such a task is difficult to accomplish, as made clear by the high percentage of dose (often exceeding 50%) depositing in the mouth and throat from many commercial inhalers (25). For cases in which the aerosol is delivered through an add-on device (or through a ventilator circuit), the analysis must be extended to include deposition in the external apparatus. *In vitro*, adult models of mechanical ventilation studying the delivery of bronchodilators from MDIs through an inline holding chamber and endotracheal tube typically measure lung deposition as less than 20% (by mass) of the delivered dose (14, 17, 18). This means that under typical ventilator conditions, approximately 80% of the aerosolized drug deposits in the holding chamber, ventilator tubing, and endotracheal tube.

Aerosol deposition on airway walls is dependant on the aerodynamic size of particles, the rate and pattern of airflow, and the geometry of the airway. In addition, deposition in the mouth and throat is greatly influenced by the type of delivery device employed (26). There exist five basic mechanisms that govern aerosol particle deposition in general, namely gravitational sedimentation, diffusion, inertial impaction, electrostatic attraction, and interception with airway walls (24). In the respiratory tract, the latter two mechanisms are usually unimportant. Electrostatic attractions between particles and walls are probably eliminated in the high humidity of the lung (4). Deposition by interception will occur when a particle entrained in the respiratory airflow comes within one particle radius of an airway wall. However, for the majority of inhaled aerosols, particle size is much less than even the smallest airway diameters, so that interception plays only a minor role in determining deposition (24). The remaining three mechanisms, sedimentation, diffusion, and impaction, determine aerosol deposition in the respiratory tract for most circumstances. They are now discussed.

2.3.1 Sedimentation

Deposition due to sedimentation occurs as a result of gravitational settling of aerosol particles onto airway walls. Therefore, a particle's likelihood for sedimentation is dependant on its time of residence in an airway, as well as its settling velocity. Settling velocity is simply the terminal velocity of a particle in still fluid, which can be determined by balancing the force of gravity experienced by the particle with the drag force in the opposite direction. For the low particle Reynolds numbers associated with

inhaled aerosols, the drag force is given by Stokes law[2]. Thus, the settling velocity may be expressed as

$$v_{\text{settling}} = \frac{C_C \rho g d^2}{18\mu} \tag{2.5}$$

where C_C — Cunningham slip correction factor;
ρ — particle density;
g — gravitational acceleration;
d — particle diameter;
μ — fluid viscosity.

The Cunningham slip correction factor is equal to unity under the continuum assumption that the particle diameter is much larger than the mean free path of the fluid. Where this assumption fails, $C_C > 1$, and may be calculated for a given particle diameter and mean free path length from formulae available in the literature (23). For a 1μm diameter spherical particle in room temperature air, $C_C \approx 1.17$, so that the Cunningham correction has only a minor effect on the settling of typical inhaled pharmaceutical aerosols, with diameters on the order of a few microns.

If the respiratory airways are imagined as a series of bifurcating cylindrical tubes, the probability that an aerosol particle will deposit by sedimentation in a particular airway can be shown to increase monotonically with the non-dimensional parameter (4)

$$t' = \frac{v_{\text{settling}} L}{UD} \tag{2.6}$$

where L — airway length;

[2] Named after George Stokes (1851). For $\text{Re}_{\text{particle}} << 1$, $\vec{F}_{\text{drag}} = -3\pi d\mu(\vec{v}_{\text{particle}} - \vec{v}_{\text{fluid}})$ gives the drag force on a sphere of diameter d in a fluid of viscosity μ acting in the direction opposite to the relative velocity of the particle.

D — airway diameter;
U — average air velocity.

By evaluating Equation 2.6, or others like it, over typical lung geometries, it can be seen that a particle's probability for gravitational sedimentation will be largest in the small airways deep in the lung (4, 24). For aerosol delivery during mechanical ventilation, sedimentation plays next to no role in determining deposition in the ventilator circuit during the inspiratory portion of the breathing cycle. The distances particles are predicted to settle over typical residence times in the holding chamber and endotracheal tube are much less than the tube diameters. However, in cases where aerosolized drug in the holding chamber is not cleared in a single inhalation (such is the case for intubated infants), gravitational settling may occur between breaths, during exhalation.

2.3.2 Diffusion

The motion of very small aerosol particles is influenced by random collisions with air molecules. Particles with diameters not much greater than the mean free path of air molecules will travel a finite distance between collisions. Over time, such particles follow nondeterministic paths, and are said to exhibit Brownian motion[3]. Brownian diffusion can lead to deposition of aerosol particles following air streamlines close to an airway wall, as in Figure 2.3. The probability that a particle will deposit by diffusion in a cylindrical tube is known to increase monotonically with the non-dimensional parameter (27, 28)

[3] Named for 19th century botanist Robert Brown, who first noticed the effect for pollen suspended in water, but most often associated with Albert Einstein, for his quantitative study in 1905.

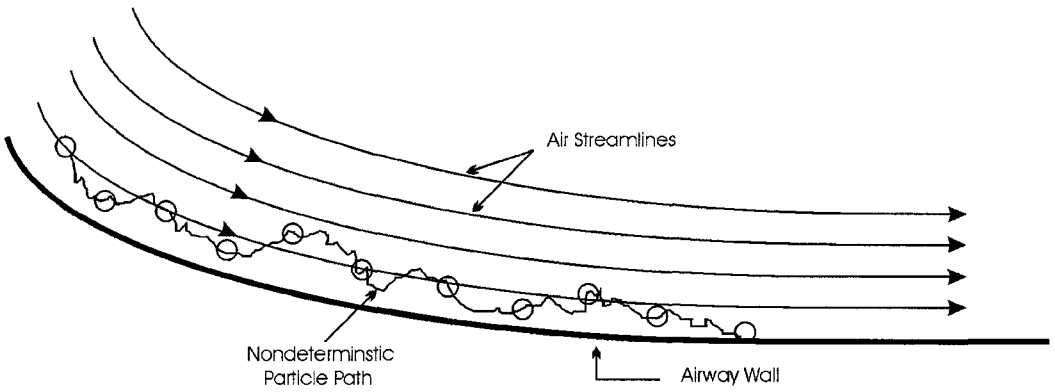

Figure 2.3 Particle deposition by Brownian diffusion.

$$\Delta = \frac{kTC_C L}{3\pi\mu d U D^2} \tag{2.7}$$

where k — Boltzmann's constant (1.38×10^{-23} J K^{-1});
T — fluid temperature;
C_C — Cunningham slip correction factor;
μ — fluid viscosity;
d — particle diameter;
L — tube length;
D — tube diameter;
U — average flow velocity through tube.

For inhaled aerosols, the probability of deposition by diffusion increases as a particle travels deeper into the lung, where airway diameters and velocities decrease. However, these conditions also favor gravitational sedimentation. From Equations 2.6 and 2.7, the probability of deposition by sedimentation is expected to decrease with decreasing particle size, while the probability of deposition by diffusion will increase with decreasing particle size. Therefore, the relative importance of diffusion in the respiratory tract will grow larger for smaller particles. Typical pharmaceutical aerosols

have MMADs of a few microns, in which case deposition in the distal regions of the lung is dominated by gravitational sedimentation. Diffusion may be non-negligible in certain cases given that polydisperse aerosol penetrating deep into the lung can contain a large number fraction of sub-micron sized particles (29). However, even in these circumstances, the majority of drug dose (by mass) is likely contained in larger, micron-scale particles, for which deposition is largely determined by sedimentation.

2.3.3 Impaction

Impaction of aerosol particles on airway walls occurs when entrained particles react too slowly to changes in the direction of airflow around bends in the respiratory tract (Figure 2.4). While aerodynamic drag forces act to continually adjust a particle's trajectory to match flow streamlines, particle inertia can pull the particle off course. Under the assumption

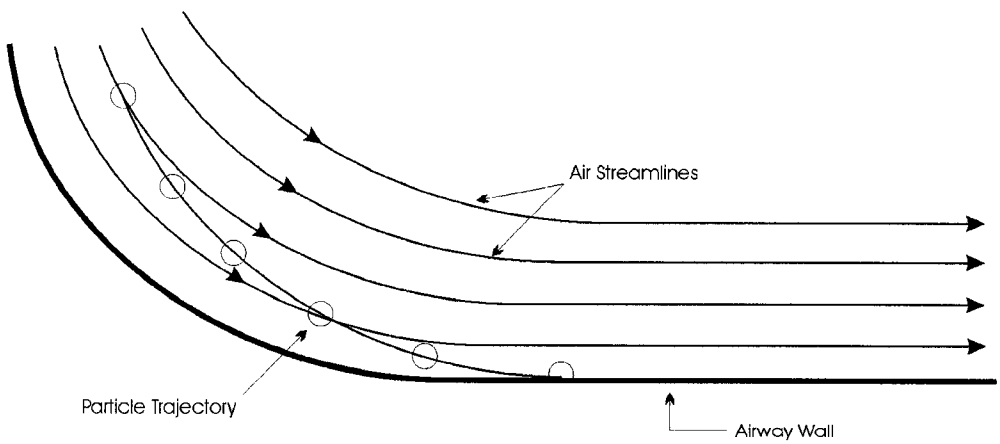

Figure 2.4 Particle deposition by inertial impaction.

that particle Reynolds numbers are small, the tendency of a particle to stray from curved streamlines is a function of the non-dimensional Stokes number

$$Stk = \frac{U\rho d^2 C_C}{18\mu D} \tag{2.8}$$

where U — average flow velocity;
ρ — particle density;
d — particle diameter;
C_C — Cunnigham slip correction factor;
μ — fluid viscosity;
D — airway diameter.

Numerous correlations from the literature predict that for a given flow pattern, the probability of particle deposition in an airway due to inertial impaction increases monotonically with Stokes number (4). Unlike deposition by sedimentation or diffusion, the probability of inertial impaction is larger for higher flow velocities. Impaction is therefore the favored deposition mechanism in the mouth, throat, and upper regions of the tracheo-bronchial airways, where flow rates are highest. In addition, the probability of inertial impaction is highly dependant on particle diameter. Particles much larger than a few microns in diameter will most often be filtered by inertial impaction in the upper or central airways before reaching more distal regions in the lung.

During mechanical ventilation, inertial impaction plays the dominant role in determining aerosol deposition in the ventilator circuit. From Equation 2.8, it is easy to see how the increased particle diameters associated with high levels of humidity during ventilation can significantly increase impaction in the holding chamber and tubing.

2.4 Particle Size Changes: Simplified Hygroscopic Theory

The tremendous importance of particle size on the deposition of inhaled aerosols has been outlined in the preceding section. Clearly, any effect on rates of change of particle size can significantly adjust the final deposition of particles in the respiratory tract. Particle size changes due to evaporation and/or condensation regularly arise during delivery of inhaled pharmaceutical aerosols; for example, in the form of growth or shrinkage of aqueous droplets delivered from nebulizers, growth of hydrophilic drug particles subject to respiratory tract humidity, or rapid evaporation of volatile propellant droplets delivered emitted by MDIs. To gain insight into the physical factors influencing evaporative and condensative particle size changes, it is instructive to consider the idealized case of a single droplet under the assumptions of simplified hygroscopic theory.

Finlay (4) outlines five assumptions that must be satisfied in order to apply the classical theory for hygroscopic growth or shrinkage of a single droplet. These are: 1) the mass transfer at the droplet surface does not cause bulk motion in the air surrounding the droplet; 2) the temperature inside the droplet does not vary spatially; 3) the motion of the particle in air is negligible; 4) the particle radius is much smaller than the mean free path of air molecules; and 5) quasi-steadiness is assumed. With these assumptions in place, classical theory is in very good agreement with experimental measurements of rates of change of droplet size (30).

Under simplified hygroscopic theory, the rate of change of droplet size is governed by diffusion of the droplet species' vapor to or from the droplet surface. If the ambient concentration of vapor in air is less than that at the surface of the droplet, the droplet will evaporate. If instead the ambient vapor concentration is greater than that at

the droplet surface, condensation will occur, and the droplet will grow. The mass flux of vapor at any point outside the droplet is given by Fick's first law of diffusion

$$j = -D\nabla c \tag{2.9}$$

where j — mass flux of vapor per unit area;
D — diffusion coefficient of droplet vapor in air;
c — mass concentration of vapor in air.

Recognizing that for the assumptions outlined above the concentration of vapor varies only with the radial distance from the center of the droplet, then multiplying Equation 2.9 by the surface area of a spherical shell centered around the droplet, and finally integrating from the droplet surface to a point far away, the rate of change of droplet mass can be determined as

$$\frac{\mathrm{d}m}{\mathrm{d}t} = -2\pi dD(c_S - c_\infty) \tag{2.10}$$

where m — mass of the droplet;
t — time;
d — droplet diameter;
c_S, c_∞ — vapor concentration at, and far away from, droplet surface.

Equation (2.10) is referred to as the Maxwell[4] equation, and is more often written in terms of droplet diameter as

[4] After James Clerk Maxwell, best known for his development of the electromagnetic theory of light, who considered the idealized problem of stationary evaporation of a spherical, motionless droplet into an infinite medium in an article entitled "Theory of the wet-bulb thermometer" written for the Encyclopedia Britannica is 1877.

$$\frac{\mathrm{d}d}{\mathrm{d}t} = \frac{-4D(c_S - c_\infty)}{\rho d} \tag{2.11}$$

where ρ — droplet density.

The vapor concentration at the droplet surface, c_S, varies rapidly (exponentially) with the temperature of the droplet. Therefore, in order to determine the rate of change of droplet size from Equation 2.10 or 2.11, the temperature of the droplet must be known. Finlay (4) derives the equation that governs the temperature of a droplet under the assumptions of simplified hygroscopic theory to be

$$-LD(c_S - c_\infty) - k_{air}(T - T_\infty) = \frac{dT}{dt}\rho c_P \frac{d^2}{12} \tag{2.12}$$

where L — latent heat of vaporization;
k_{air} — thermal conductivity of air;
c_P — specific heat capacity of the droplet;
T_∞ — ambient temperature far from the droplet;
T — droplet temperature.

The three terms making up Equation 2.12 represent (from left to right) the energy lost or gained by the droplet due to evaporation or condensation, heat flux to or from the droplet, and changes in the internal energy of the droplet. It is well known that the temperature of a droplet introduced to a new environment will quickly correct to a constant steady-state (24), or 'wet-bulb' (4), temperature. The term on the right hand side of Equation 2.12 represents this transient temperature adjustment. For steady-state evaporation or condensation, the right hand side of Equation 2.12 can be set to zero and the remaining terms solved iteratively (note that c_S is dependant on droplet temperature)

for the wet-bulb droplet temperature. With the transient term neglected, Equation 2.12 can be shown to be identical to the equation for droplet temperature during stationary evaporation derived by both Maxwell (31) and Fuchs (30).

Once known, the wet-bulb droplet temperature may be used in determining the saturation vapor concentration at the droplet surface, which in turn is required to calculate the rate of change of droplet size from Equation 2.10 or 2.11. While it should be noted that such an analysis ignores any size changes occurring during the period of transient temperature adjustment, Finlay (4) has shown that for evaporating water droplets in room or body temperature air, the transient term in Equation 2.12 may be neglected with little consequence to droplet lifetimes.

2.5 Particle Size Changes: Stefan Flow

Simplified hygroscopic theory proves an excellent tool in analyzing evaporation of droplets of water or similar liquids. However, the theory may not be applied to the evaporation of liquefied gases, such as the HFA propellants found in MDIs, due to violation of the assumption of no bulk motion in the gaseous phase surrounding the droplet. The vapor pressure of propellant droplets is much higher than that of water, so that evaporation can occur at such a rate as to establish a convective motion in the vapor/air mixture away from droplet surfaces, known as Stefan flow[5]. The requirement for such a flow to exist in cases in which the vapor pressure of the droplet is non-negligible compared to atmospheric pressure can be established through consideration of the partial pressure gradient of the vapor (Figure 2.5), as described by Fuchs (30). To

[5] First shown by J. Stefan in 1881.

maintain constant atmospheric pressure in the vapor/air mixture, the vapor pressure gradient must be balanced by an equal and opposite gradient of the partial pressure of air. The latter gradient requires air to diffuse towards the droplet surface; however, as air cannot penetrate the surface, the net flux of air towards the droplet should be zero. Therefore, to compensate for the diffusion of air *towards* the droplet surface, a convective flow must exist *away* from the droplet surface. This flow carries not only air, but also droplet vapor away from the surface, so that the rate of evaporation is greater than that which would be predicted with Stefan flow neglected.

Determining the rate of change of size for a droplet exhibiting Stefan flow requires the solution of a boundary volume problem involving coupled first- and second-order ordinary differential equations governing the vapor mass fraction and droplet temperature, respectively (4). Solutions to the problem may be obtained through numerical methods, or, with some assumptions, through an analytical solution available

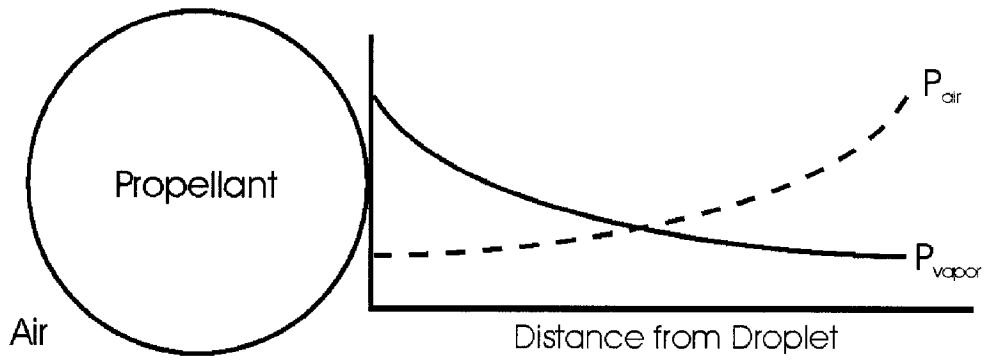

Figure 2.5 Pressure gradients in an air/vapor mixture with distance from the droplet surface.

in the literature on combustion of sprays (32), and described by Finlay (4) for analysis of propellant droplets. Propellant evaporation models have been built into theoretical analyses of the spray issued from an MDI by both Clark (33) and Dunbar (34). While these authors have provided great insight into the production and behavior of MDI sprays, such models are limited in their prediction of post-nozzle evaporation of propellant droplets for a number of reasons.

First, propellant droplets exit the MDI nozzle in a high speed jet of vapor, which rapidly mixes with coflowing ambient air. The evaporation of propellant is two-way coupled, in that evaporation affects the temperature and vapor concentration in the surrounding air, which in turn affect the rate of evaporation. Dunbar (34) concluded that the inadequacy of his evaporation model was associated with an inability to represent the temperature and vapor concentration in the air surrounding droplets emitted from an MDI.

In addition to this difficulty, the fact that droplets leave the exit nozzle at high velocity requires that the effect of convection should be included in determining rates of evaporation. However, initial droplet diameters and velocities leaving the nozzle are difficult to measure with existing optical technologies due to spatial variations in the refractive index of the vapor-air mixture and to the small length scales over which droplet evaporation and deceleration progress (34). While various authors report exit velocities of approximately 25-30 m/s (35), Dunbar's model (34) predicts exit velocity from an HFA 134a MDI to decrease from a maximum of 225 m/s over the course of an actuation.

As a consequence of the difficulties associated with experimental measurement of droplet sizes near exit nozzles, little data exists for the rates of change of size of

propellant droplets produced from an MDI. With such limited data available, validation of evaporation models is difficult. At best, theoretical models of evaporation, which include the effect of Stefan flow, can provide predictions of the time scales over which MDI droplet evaporation should occur. However, these predictions are highly dependent on determination of the temperature and propellant vapor concentration of the surrounding air.

Chapter 3

Experimental Design and Procedures

3.1 Single Droplet Experiments for Measuring Propellant Evaporation from MDI Formulations

Evaporation of propellant from MDI aerosols rapidly reduces droplet diameters downstream from the exit nozzle. However, the presence of excipients in the MDI formulation, or water vapor in the surrounding air, may decrease the rate of propellant evaporation. Gupta et al. (36) have recently reported large reductions in fine particle fraction (defined as the fraction of the total aerosol mass contained in droplets of diameter < 4.7 μm) as the cosolvent concentration in solution MDI formulations was increased. These results were attributed to a retarded evaporation of propellant-cosolvent droplets (36). During mechanical ventilation, the reduced drug delivery observed when MDIs are actuated into warm, humid airflow is often attributed to a reduction in the evaporation rate of propellant droplets, as was discussed in Section 1.3. Lange and Finlay (19) have suggested that a barrier to propellant evaporation may be formed at droplet surfaces through interactions between surfactant molecules, which stabilize MDI drug suspensions, and water molecules in the surrounding air.

The influence of formulation on the rate of evaporation of propellants is not easily evaluated, owing to the difficulty of obtaining quantitative aerosol size measurements near the MDI exit nozzle (see Section 2.5). As an alternative approach, propellant evaporation may be better studied through examination of an isolated propellant-air interface, as provided by a single droplet experiment. Lin and Gentry (37) have noted

several limitations often associated with single droplet experiments for examining vaporization of sprays, including that experimental droplet diameters are orders of magnitude larger than typical spray droplets, and that the droplet suspension device provides a heat source and a site for vapor bubble nucleation. However, these authors defend the methodology, noting that size changes progress more slowly for larger droplets, so that time scales become experimentally feasible (37). Furthermore, droplets with volume of the order of 1 μl may be studied with an optical microscope, as opposed to scanning or transmission electron microscopes (37). While concerns about conduction of heat down the droplet suspension device are valid, the present study compared evaporation rates of various formulations obtained from an identical experimental apparatus and procedure, so that any relative difference in evaporation between formulations could not be attributed to the suspension device. With these considerations, single droplet experiments may provide an inexpensive means through which to study propellant evaporation for various MDI formulations. In consistency with the thesis, such experiments were performed to examine the evaporation of HFA propellant formulations in the warm, humid conditions typical during mechanical ventilation.

3.1.1 Materials

Initial experiments were performed using HFA 227ea propellant (Dymel® 227ea/p; DuPont Fluorochemicals, Wilmington, DE), chosen in place of the more volatile HFA 134a in an effort to slow down evaporation of suspended droplets. Ethanol (anhydrous ethanol; Commercial Alcohols, Brampton, ON) cosolvent and sorbitan trioleate (Span®85; Sigma-Aldrich, St. Louis. MO) surfactant were studied as excipients.

Formulations of pure propellant; propellant and 15% w/w ethanol (typical of solution MDI formulations); and propellant, 15% w/w ethanol, and 0.2% w/w sorbitan trioleate (typical of suspension formulations) were prepared. No drug was included in the formulations studied, as drug concentrations are typically less than a few tenths of 1% (by weight). At these concentrations, drug, whether in suspension or solution, is expected to have very little effect on propellant evaporation.

3.1.2 Apparatus and Procedures

A schematic of the experimental setup can be seen in Figure 3.1. Droplets were suspended into a conditioned viewing chamber (50 mm x 45 mm x 25 mm) from a large-gauge needle with inner diameter of 2.5 mm (#91010; Hamilton Company, Reno, NV). Formulation was supplied to the needle through a 250 µl syringe (Gastight® #1725; Hamilton Company, Reno, NV). All apparatus involved in the transfer of formulation to

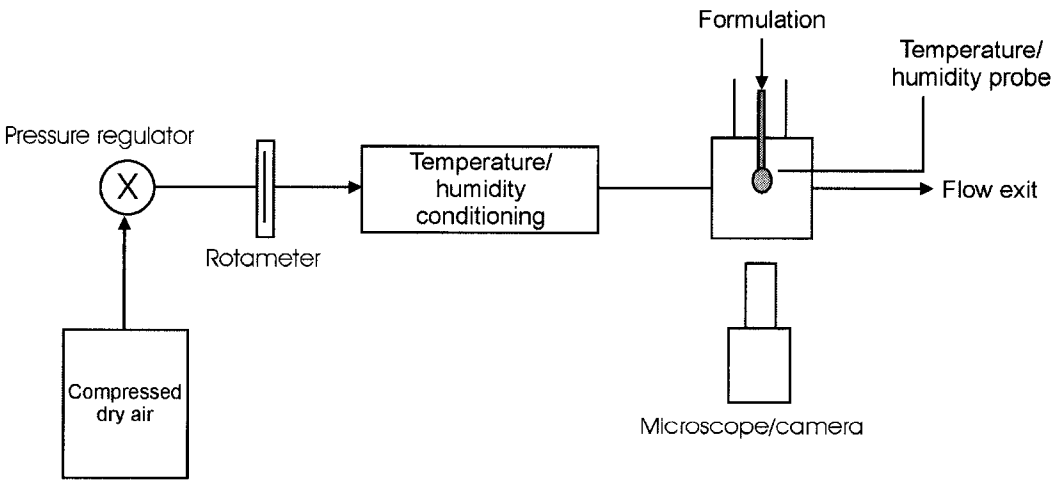

Figure 3.1 Schematic of the experimental apparatus for pendant droplet experiments.

the syringe was cooled with dry ice well below the propellant boiling point (-15.6° C at 1 atm) so as to limit vaporization of the propellant prior to suspension of droplets in the viewing chamber. In addition, the syringe was held above the viewing chamber in an insulated plastic cylinder packed with dry ice, which created a column of formulation above the suspended droplet (Figure 3.2). For each experimental run, only a small amount of the formulation (<10%) available in the syringe was suspended as droplets, to avoid significantly increasing the concentration of excipients as the volatile propellant vaporized.

The present experimental design differed from many traditional pendant droplet experiments, in which isolated spherical droplets are grown at the ends of extremely thin

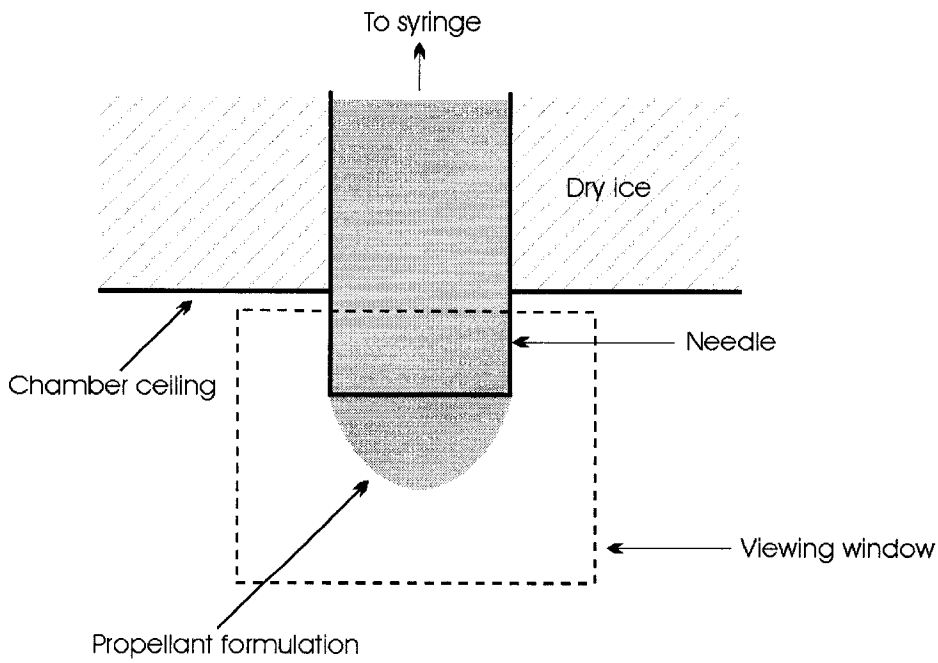

Figure 3.2 Schematic of droplet suspension into the viewing chamber.

capillaries or filaments (37). The surface tension of HFA 227ea is sufficiently low (~7.5 mN/m at 20° C compared to 72.8 mN/m at 20° C for water) to severely limit the size of spherical droplets that can be suspended from such devices. As discussed in the introduction to Section 3.1, droplets with volumes of the order of 1 μl were required for measurement with the available imaging system. The suspension rig pictured in Figure 3.2 allowed for much larger, albeit non-spherical and non-isolated, droplets to be studied. Such a design was sufficient in allowing for comparison of relative rates of evaporation from a propellant-air interface between different propellant formulations.

Temperature and humidity were controlled in the viewing chamber through a steady flow of conditioned air. A low flow rate of 0.5 l/min was maintained with a single-stage pressure regulator (Praxair, Danbury, CT) and monitored with a 0-10 l/min rotameter (Omega Canada, Laval, QC) to ensure that effects of the fluid motion on heat and mass transfer at the droplet surface were kept minimal. Temperature and humidity conditioning of the airflow was achieved through a heated respiratory humidifier (MR 370; Fisher & Paykel Healthcare, Laguna Hills, CA), and monitored in the viewing chamber with a temperature/humidity probe (RH30C; Omega Canada, Laval, QC) with accuracies of ± 0.3° C and ± 3% relative humidity (RH).

For each of the three formulations studied, four experimental runs were performed for both dry (< 10% RH) and humid (100% RH) conditions, at 37 ± 2° C. The syringe was filled at the start of each run, and then five 5 μl droplets were suspended, in succession, into the viewing chamber, with a pause of approximately five seconds between the complete evaporation of a droplet and the introduction of the next.

3.1.3 Digital Image Processing

Droplet evaporation was recorded through a microscope-coupled CCD camera (#4915; Cohu, San Diego, CA) at 16x magnification. Vertical and horizontal scale factors between image pixels and physical lengths were determined from images (at the same magnification) of a grid with known spacing between vertical and horizontal lines. In-house frame capture software recorded the elapsed time between image frames. On average, about seven frames were captured per second. For each image, the droplet profile was obtained through analysis of grayscale image intensity gradients, according to Axisymmetric Drop Shape Analysis (ADSA) routines (38).

An existing FORTRAN computer program, which carries out the droplet profile detection routine developed by Cheng for use in ADSA (39), was available in the laboratory in which experiments were performed. This program employs a gradient method to determine the coordinates of the droplet profile. Such methods take advantage of the rapid change in gray level at the edge of a drop. In the existing program, the Sobel edge operator (38) is applied at every pixel of the droplet image to produce a gradient image. The coordinates of the droplet profile are then determined by searching the gradient image for local maxima.

The ADSA technique proceeds to fit the droplet profile coordinates to a Laplacian curve, defined by the Laplace equation of capillarity (38). The Laplace equation represents the balance between surface tension and external forces, namely gravity, for a droplet in mechanical equilibrium; therefore, with the shape of the profile known, the surface tension can be determined. However, in the present study, it is only the droplet volume, not the surface tension, which is required. Moreover, the Laplace equation does

not apply to rapidly evaporating propellant droplets, as mechanical equilibrium is not established. Consequently, a separate FORTRAN code was written for the purpose of calculating droplet volumes directly from the droplet profile coordinates.

Droplet volumes were calculated by numerical integration of the profile coordinates. However, in many cases, gaps existed in the droplet profile returned by the gradient method, due to reflection of ambient light off the droplet, or to poorly focused droplet edges, as was the case for the profile displayed in Figure 3.4(A). Therefore, to limit errors in volume calculation associated with incomplete profiles, the profile coordinates returned by the gradient method were fit with a second order polynomial through least-squares regression. A complete axisymmetric profile, ranging from the suspending needle to the droplet low-point with no gaps, was then generated from the fitted polynomial. Figures 3.3 and 3.4 display (A) the droplet profile coordinates returned by the gradient method, and (B) those generated by the subsequent polynomial fit. Whether the original coordinates represent the droplet profile completely, as in Figure 3.3(A), or only in part, as in Figure 3.4(A), the coordinates produced by the best-fit polynomial follow the droplet profile very closely.

In order to determine the droplet volume for a given image frame, the generated profile coordinates were rotated 180°, and a cylindrical coordinate system was introduced, as in Figure 3.5. Referring to Figure 3.5, z' and r' represent arrays holding the profile coordinates in the z and r directions, respectively. Therefore, the coordinates of the i^{th} point on the droplet profile are given by $[z'(i), r'(i)]$. Droplet volume was then determined by integration.

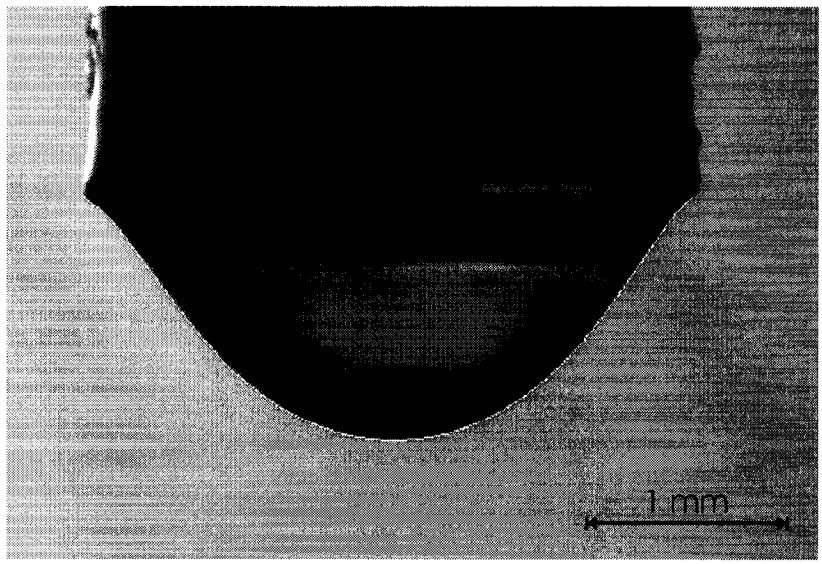

(A)

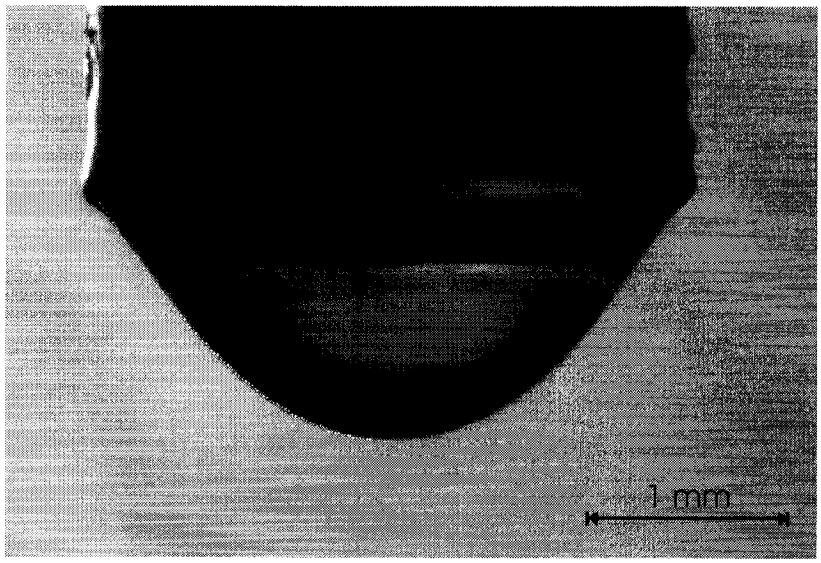

(B)

Figure 3.3 Suspended HFA 227ea droplets with superimposed profile coordinates (shown in white) returned by (A) the gradient method, and (B) the subsequent polynomial fit.

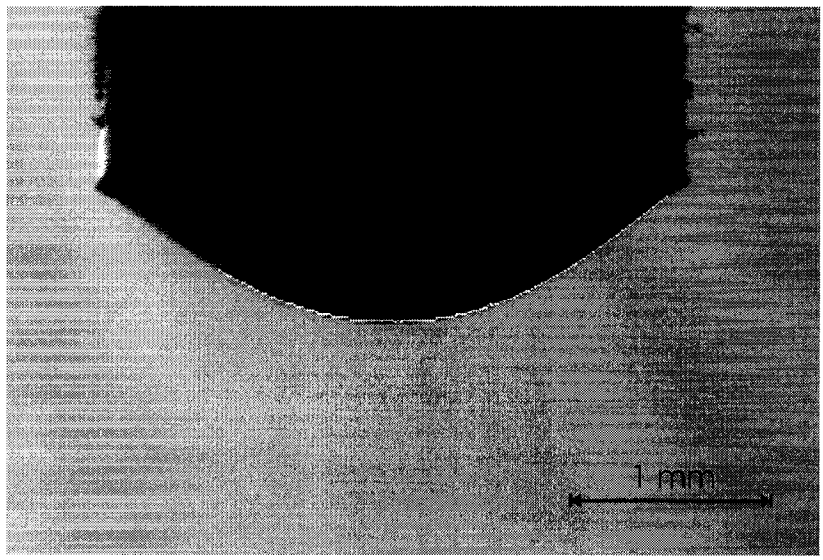

(A)

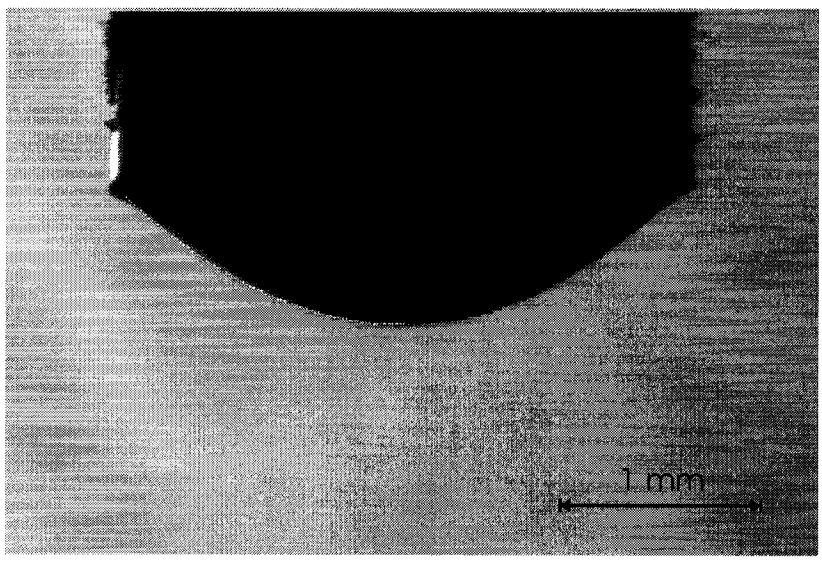

(B)

Figure 3.4 Suspended HFA 227ea droplets with superimposed profile coordinates (shown in white) returned by (A) the gradient method, and (B) the subsequent polynomial fit.

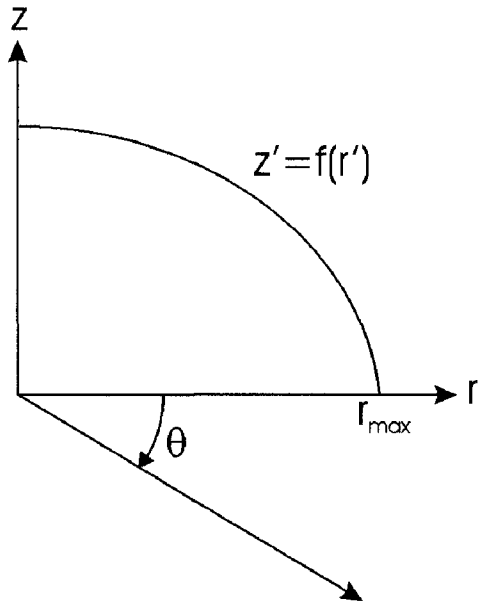

Figure 3.5 The droplet profile is rotated 180° and a cylindrical coordinate system is introduced in order to determine droplet volume by integration. *z'* and *r'* are arrays holding the profile coordinates in the z and r directions.

With the assumption of an axisymmetric droplet shape, droplet volume was determined from the profile pictured in Figure 3.5.

$$V = \iiint_V \mathrm{d}V \tag{3.1}$$

$$V = \int_0^{2\pi} \int_0^{r_{max}} \int_0^{f(r')} r' \mathrm{d}z \mathrm{d}r \mathrm{d}\theta \tag{3.2}$$

$$V = 2\pi \int_0^{r_{max}} r' f(r') dr \tag{3.3}$$

where r_{max} is the last entry contained in the array *r'*.

Equation 3.3 was numerically integrated using the extended trapezoidal rule (40) to yield droplet volume. In such a manner, the volume of the droplet in each image frame was calculated, so that volume versus time data was recorded for each evaporating droplet.

3.1.4 Statistical Analysis

Mean rates of droplet evaporation were compared between the three formulations studied, and, for individual formulations, between dry and humid conditions. Statistical comparisons were made using non-directional *t*-tests for independent samples, with a significance level of $p = 0.05$.

3.2 Bench Testing of MDI Aerosol Deposition in a Mechanical Ventilation Holding Chamber

It is well established that the humid airflow present during mechanical ventilation leads to increased MDI aerosol deposition in the holding chamber and ventilator tubing (see Section 1.3). However, the majority of studies make no attempt to determine the size distribution of the aerosol at any point in the ventilator circuit. Of the few that do (for example, Lange and Finlay (19)), the aerosol is sampled at the distal end of the endotracheal tube. Such measurements give a good indication of the size of particles delivered to the patient; however, they give no indication of the increased particle sizes that are thought to elevate aerosol deposition in the holding chamber and tubing in the presence of humidity. Indeed, Lange and Finlay (19) found no significant difference between dry (8% RH at 37° C) and humid (100% RH at 37° C) conditions in the particle

size distribution of MDI aerosols measured distal to the endotracheal tube in an *in vitro* model of mechanical ventilation. Apparently, any effect of humidity on the evolution of particle sizes within the ventilator circuit had run its course by the point at which the aerosol was sampled.

In the present study, a bench test was designed to examine inertial impaction of MDI aerosols in a mechanical ventilation holding chamber. Additionally, particle size distributions were measured at two distances from the holding chamber exit in an effort to observe the rate and direction (growth or shrinkage) of size changes distal to the device. Such data is necessary for evaluating existing explanations of the increased deposition of MDI aerosols in the confined, humid environment of the ventilator circuit.

3.2.1 Apparatus and Procedures

The experimental apparatus is pictured schematically in Figure 3.6. Temperature and humidity conditions were maintained within a large climatized chamber (0.67 m^3; Hotpack, Waterloo, ON). Particle size measurements were made with an eight-stage cascade impactor (Mark II Andersen Impactor; Thermo Andersen, Smyrna, GA). Such a device relies on inertial impaction of aerosol particles on a series of plates or 'stages' (Figure 3.7). The stages are designed to filter out progressively smaller particle sizes, generally by decreasing the nozzle size or reducing the distance between the nozzle and plate. The cutoff size of each stage can be calibrated for a given flow rate through the device, and is conventionally expressed as the d_{50} value, the aerodynamic diameter for which 50% of particles would collect on the plate. For the Mark II Andersen Impactor,

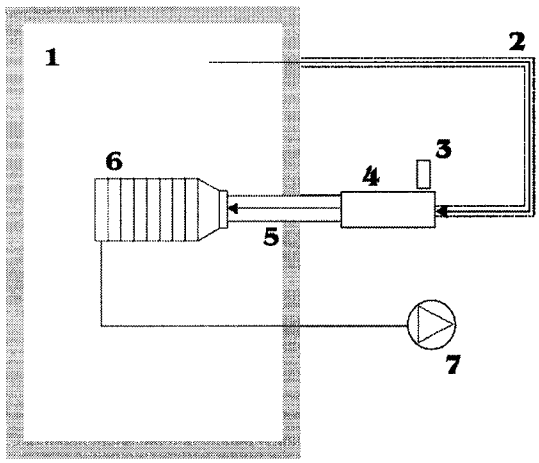

Figure 3.6 Schematic diagram of the bench test: **1** climatized chamber; **2** insulated inspiratory tubing; **3** MDI canister; **4** holding chamber; **5** tygon tubing; **6** cascade impactor; **7** vacuum pump (28.3 l/min).

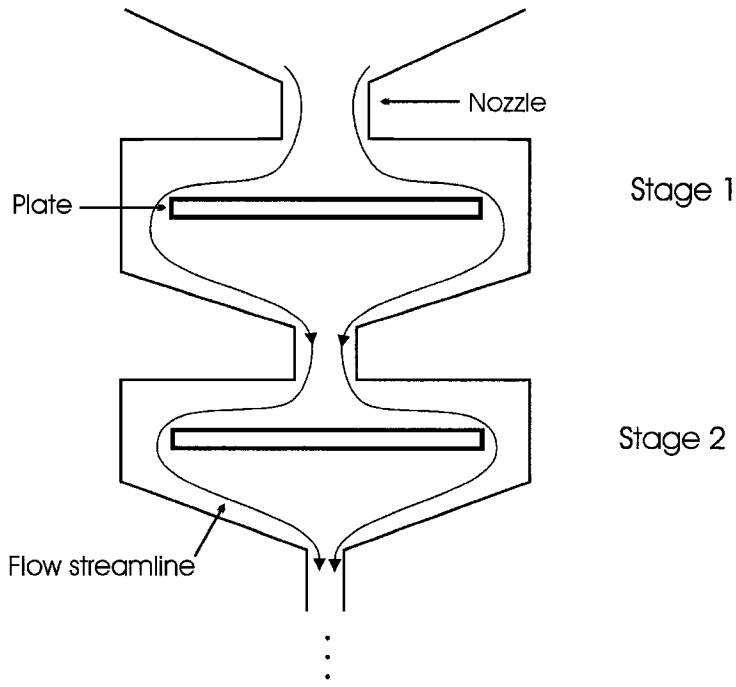

Figure 3.7 Schematic of the first two stages of a cascade impactor.

operated at a flow rate of 28.3 l/min, the value of d_{50} for each impactor stage is given in Table 3.1.

TABLE 3.1

CUTOFF DIAMETERS FOR MARK II ANDERSEN IMPACTOR

Stage	d_{50} (μm)
0	9.0
1	5.8
2	4.7
3	3.3
4	2.1
5	1.1
6	0.7
7	0.4

In conducting the present experiments, the cascade impactor was positioned inside the climatized chamber so as to establish thermal equilibrium with the conditioned air, thereby eliminating adverse effects on particle sizing associated with heat transfer to or from the impactor walls (41). The horizontal orientation of the impactor is known not to alter its particle size selection (23).

Conditioned air was drawn through the holding chamber (Aerochamber® MV; Trudell Medical Inernational, London, ON) via insulated tubing. A tygon tube with inner diameter of 1.9 cm connected the holding chamber to the impactor. This tube was kept straight so as to minimize deposition of MDI aerosol between the holding chamber and the impactor. Particle size distributions were measured using tubing with lengths of 15 cm and 45 cm, so as to study the time dependency of sizes downstream from the holding

chamber. A vacuum pump maintained a constant flow rate of 28.3 l/min throughout the experimental circuit.

Two commercially available salbutamol sulphate MDI formulations, characterized in Table 3.2, were investigated. One of the formulations (Airomir®, 100 μg salbutamol/puff; 3M Canada, London, ON) was representative of the majority of current MDI formulations, in that it contained cosolvent and surfactant constituents. The other (Ventolin® HFA, 100 μg salbutamol/puff; GlaxoSmithKline Canada, Mississauga, ON) contained only the drug suspended in propellant, with no excipients.

TABLE 3.2

SALBUTAMOL SULPHATE MDI FORMULATIONS

	Airomir®	Ventolin® HFA
Propellant:	HFA 134a	HFA 134a
Drug Form:	suspension	suspension
Cosolvent:	ethanol	none
Surfactant	oleic acid	none

Experiments were performed for each formulation in both dry (37° C, ≤ 10% RH) and humid (37° C, 100% RH) conditions, with each length of tubing. The temperature and humidity in the climatized chamber were monitored with a portable thermohygrometer (HI 8564; Hanna Instruments, Limena, Italy) with accuracies of ± 0.4° C and ± 2% RH. In all experiments, the temperature was held inside the range of 37 ± 2° C. The relative humidity remained within 8 ± 2% RH during dry experiments, and

typically fluctuated between 98% and 100% RH during humid experiments, not falling below 96% RH at any time.

Prior to each experiment, the MDI canister was primed by firing three times into the ambient air. The MDI was then actuated five times into the holding chamber, with a 30 sec pause between actuations. The MDI canister was shaken for 10 sec preceding every actuation. Between experiments, the MDIs were stored on their sides at room temperature.

Initial experiments were performed with the 15cm tubing connecting the holding chamber to the cascade impactor. For each combination of MDI formulation and humidity condition, the experiment was repeated five times (n = 5). Due to the consistency of the data, the number of repetitions was reduced to three (n = 3) when the length of tubing was increased to 45 cm.

3.2.2 Assay Technique

The amounts of salbutamol sulphate deposited in the holding chamber, the tubing, and the cascade impactor plates were assayed following each experiment. Both the holding chamber and the tubing were washed with 10 ml of distilled water. The impactor plates were washed with either 5 ml or 10 ml of distilled water, according to the expected amount of drug on a plate. The concentration of salbutamol sulphate in each solution was then determined from measurement of its absorbance by ultraviolet spectrophotometery (8452A; Hewlett-Packard, Palo Alto, CA) at $\lambda = 224$ nm. For calibration, the absorbance of a standard solution of salbutamol sulphate (Sigma Chemicals, St. Louis, MO) was measured prior to each set of assays.

3.2.3 Statistical Analysis

Least-squares regression was used to fit cascade impactor data from each experiment with a log-normal distribution, thereby obtaining the mass median aerodynamic diameter (MMAD) and the geometric standard deviation (GSD) of the MDI aerosol. The MATLAB script file written to accomplish this curve fitting can be found in Appendix C. The amounts of drug depositing in the holding chamber and tubing were expressed as percentages of the total mass delivered from the MDI during an experiment. Statistical comparisons between results were made through the calculation of *t*-ratios for independent samples. In determining statistical significance, critical values of t were those pertaining to a non-directional, two-tailed test, with the exception of comparisons of holding chamber deposition from the same MDI formulation, where the directional hypothesis that deposition increases with humidity allowed for one-tailed values to be used.

Chapter 4

Experimental Results

4.1 Results from Single Droplet Experiments

Prior to performing experiments with volatile propellant droplets, initial validation data was collected for water droplets with volumes of 2.5 μl and 5 μl as measured by graduations on the syringe. The ability of the image processing routine to accurately determine the volume of the suspended water droplets was tested. Table 4.1 compares the droplet volumes determined from the syringe graduations to those measured through image processing.

TABLE 4.1

VOLUMES OF WATER DROPLETS FOR VALIDATION OF IMAGE PROCESSING

Volume from Syringe Gradients (μl)	Volume from Image Processing (μl)
2.50	2.62
2.50	2.58
2.50	2.69
5.00	5.53
5.00	5.34
5.00	5.22

A discrepancy of less than 11% was recorded between droplet volumes as determined through image processing and those measured from syringe graduations. The volumes determined through image processing were systematically larger than those measured from syringe gradients. Such a trend may result from error in the specification

of the vertical position of the needle (which must be input by the user) in the image file, or from human error in reading the syringe graduations. Alternatively, it is possible that a small volume of water suspended from the tip of the needle due to surface tension before each droplet was formed added to the total volume of the droplet. In this case, the image processing may actually be reporting a value closer to the true volume of the suspended drop than that measured from syringe graduations. Whatever the cause of the discrepancy, the data from Table 4.1, along with visual evidence of the accuracy of the image processing routine in determining droplet profiles (see Figures 3.3 and 3.4), suggests that the image processing routine provides reasonable estimates of the volume of suspended droplets for comparison of droplet size changes between propellant formulations.

The low surface tension and high vapor pressure of the propellant resulted in flat droplet profiles, with a limited range of observable droplet volumes, from ~4 μl to ~1 μl. Typical volume versus time data for an evaporating propellant droplet is shown in Figure 4.1. Over the range of volumes available, the rate of change of droplet volume with time can be approximated as linear. Such an approximation allowed for the rate of droplet evaporation to be expressed in terms of a single variable, that being the slope of the linear least-squares fit to the data. Mean droplet evaporation rates (n = 20) for each formulation, in both dry and humid conditions at 37° C were obtained, and are given in Figure 4.2. No significant difference ($p > 0.1$) was observed in the rate of droplet evaporation between dry and humid conditions, regardless of the formulation. In addition, comparisons between pure propellant and propellant-ethanol formulations

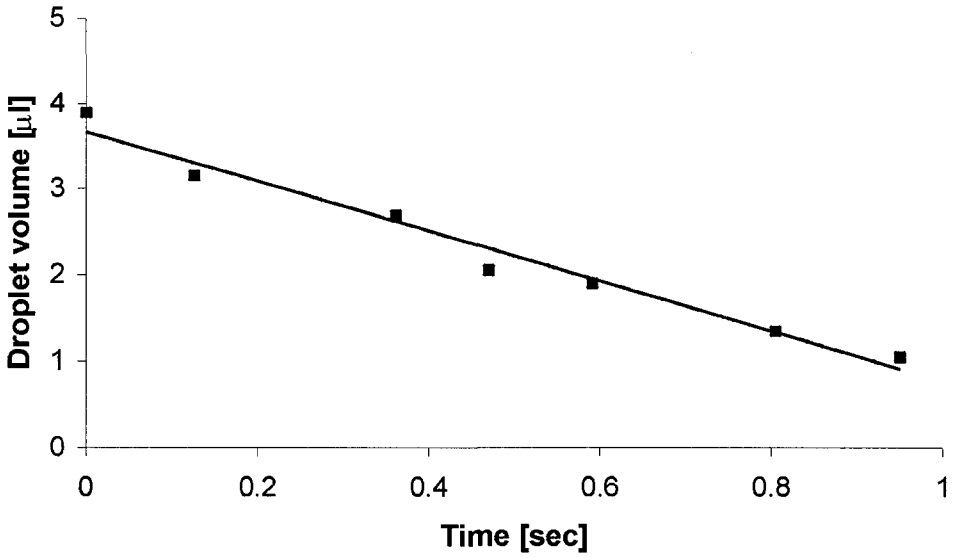

Figure 4.1 Volume versus time data for an evaporating droplet of pure HFA 227ea propellant at 37° C and <10% RH. Line represents a linear least-squares fit of slope –2.9µl/sec (R^2 = 0.9729).

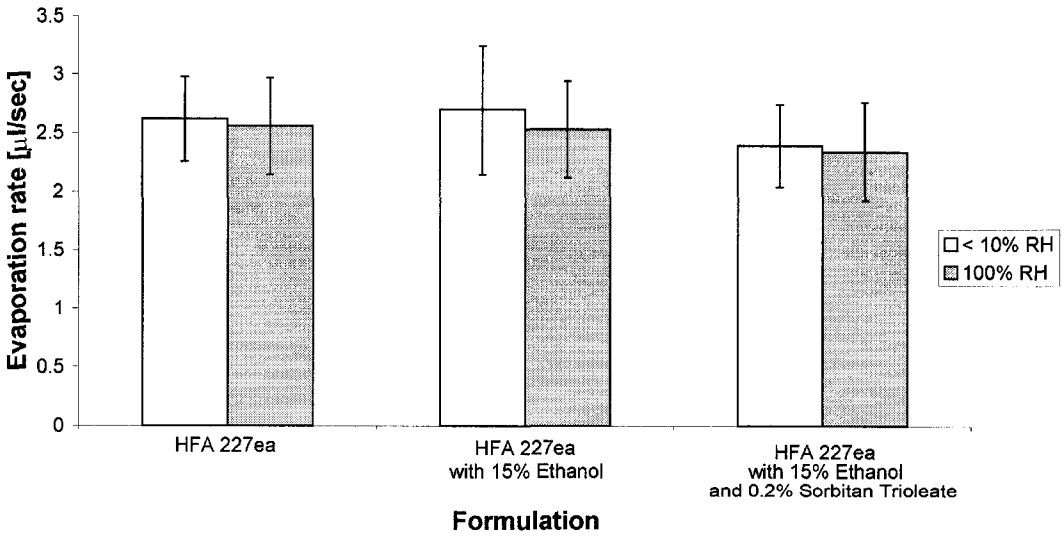

Figure 4.2 Mean evaporation rates for suspended droplets of HFA 227ea formulations in both dry and humid conditions (n = 20). Error bars represent one standard deviation.

yielded no significant difference ($p > 0.1$) in droplet evaporation rate in dry or humid conditions. For either humidity level, evaporation rates of the propellant-ethanol-surfactant formulation appear to drop off slightly from those for the other two formulations, though the difference is only marginally significant (p between 0.05 and 0.1).

Volume versus time data, and the corresponding linear least-squares fit, for each of the droplets from which the mean values displayed in Figure 4.2 were calculated is given in Appendix A.

4.2 Results from Holding Chamber Bench Tests

The bench tests were designed so that aerosol deposition in the tubing used to separate the holding chamber and cascade impactor was kept minimal. Indeed, in all cases, the amount of drug depositing in the tubing was $\leq 2\%$ of the total deposition.

The mean percentage of drug depositing in the holding chamber under dry and humid conditions is compared for both lengths of tubing for the Airomir® formulation in Figure 4.3, and for Ventolin® HFA in Figure 4.4. As expected, deposition in the holding chamber is independent of the length of tubing separating it from the impactor. For both dry and humid conditions, the holding chamber deposition was significantly higher ($p < 0.05$) for the Ventolin® HFA formulation than for the Airomir® formulation. In addition, deposition in the holding chamber increased between dry and humid conditions for both formulations. This result was statistically significant ($p < 0.05$) for all cases, with the exception of the Ventolin® HFA formulation with 45 cm tubing, in which case

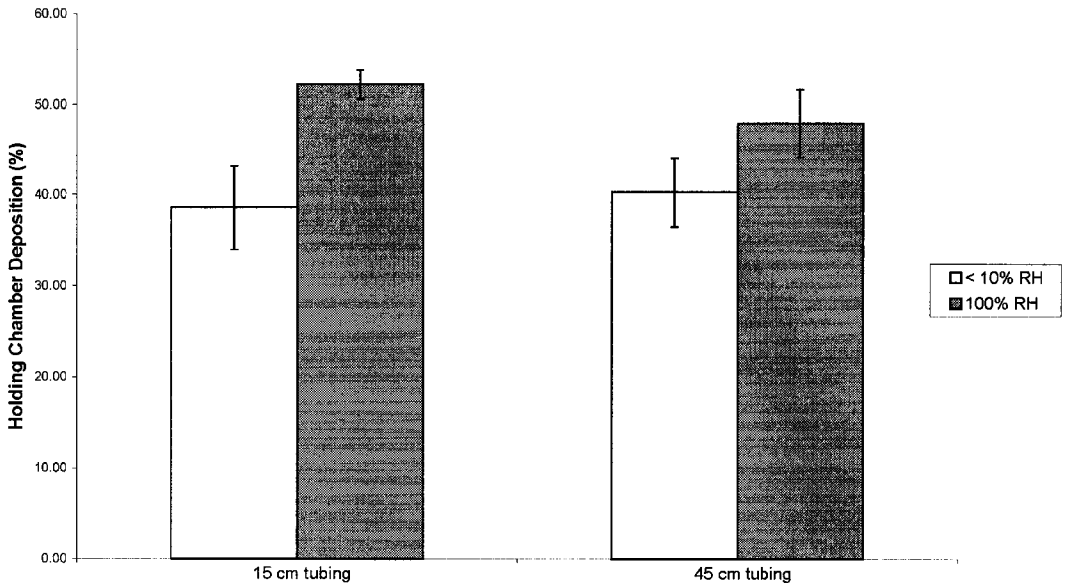

Figure 4.3 The percentage of drug depositing in the holding chamber from the Airomir® MDI in dry compared to humid airflow. Results are shown for experiments with two different lengths of tubing separating the holding chamber from the cascade impactor. Error bars represent one standard deviation.

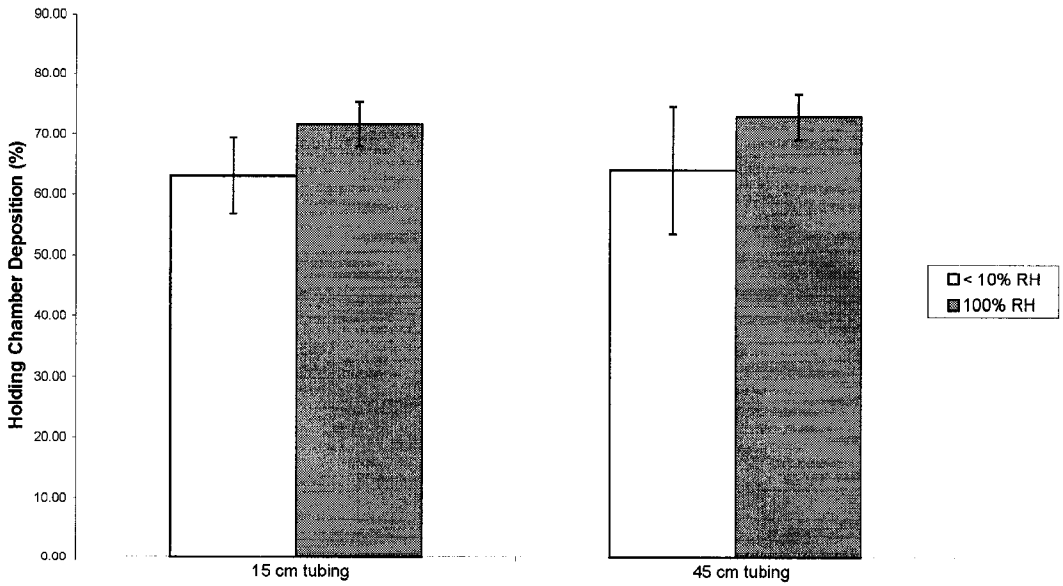

Figure 4.4 The percentage of drug depositing in the holding chamber from the Ventolin® HFA MDI in dry compared to humid airflow. Results are shown for experiments with two different lengths of tubing separating the holding chamber from the cascade impactor. Error bars represent one standard deviation.

the large standard deviation recorded for the dry condition prevented statistical significance.

For each experimental run, the particle size data measured by the cascade impactor was fit with a log-normal distribution by least-squares regression, in order to determine the MMAD and GSD of the aerosol. Tables 4.2 and 4.3 give the mean values of MMAD and GSD for the Airomir® and Ventolin® HFA MDIs, respectively, in dry and humid conditions, measured at either distance downstream from the holding chamber.

For either formulation, MMAD was observed to increase significantly ($p < 0.01$), nearly doubling, between dry and humid conditions. For dry conditions, no significant difference ($p > 0.1$) in particle size was detected when the distance between the holding chamber and cascade impactor was increased from 15 cm to 45 cm. This result suggests

TABLE 4.2

PARTICLE SIZE DISTRIBUTIONS OF AEROSOL FROM AIROMIR® MDI DOWNSTREAM FROM THE HOLDING CHAMBER UNDER DRY AND HUMID CONDITIONS AT 37° C

Tubing Length (cm)	RH (%)	MMAD (μm)	GSD
15	< 10	1.93 ± 0.11	1.41 ± 0.11
15	100	3.72 ± 0.05	1.23 ± 0.01
45	< 10	1.97 ± 0.09	1.29 ± 0.14
45	100	3.52 ± 0.12	1.36 ± 0.04

Results are expressed as mean ± standard deviation.

TABLE 4.3

PARTICLE SIZE DISTRIBUTIONS OF AEROSOL FROM VENTOLIN® HFA MDI DOWNSTREAM FROM THE HOLDING CHAMBER UNDER DRY AND HUMID CONDITIONS AT 37° C

Tubing Length (cm)	RH (%)	MMAD (μm)	GSD
15	< 10	2.01 ± 0.09	1.49 ± 0.03
15	100	3.85 ± 0.12	1.25 ± 0.02
45	< 10	1.92 ± 0.15	1.51 ± 0.03
45	100	3.60 ± 0.10	1.38 ± 0.08

Results are expressed as mean ± standard deviation.

that in dry airflow, final particle sizes (i.e. those of the suspended drug and any other nonvolatile components) had been reached prior to the measurements at either distance. Conversely, under high relative humidity, MMAD decreased significantly ($p < 0.05$) and GSD increased significantly ($p < 0.05$) for both formulations as the distance to the impactor was increased. Such data provides quantitative evidence of the rate and direction of particle size changes downstream from the holding chamber.

Values of percentage holding chamber deposition, MMAD, and GSD for each experimental run may be found in Appendix B.

Chapter 5

Analysis of Data

5.1 Single Droplet Experiments

The single droplet study found no difference in the rate of evaporation of HFA 227ea formulations between dry and humid conditions. Such a result casts doubt on the hypothesis proposed by previous authors that retarded propellant evaporation is responsible for changes in aerosol deposition when MDIs are actuated into warm, humid airflow during mechanical ventilation. Indeed, it is unlikely that water molecules in the surrounding air will have an appreciable presence at droplet surfaces, as HFA propellants have little affinity for water (Table 5.1). Furthermore, though very cold, droplet surfaces change rapidly as propellant evaporates, making them poor sites for water vapor condensation.

TABLE 5.1

WATER SOLUBILITY IN HFA PROPELLANTS AT 25° C

Propellant	Water Solubility (w/w)
HFA 134a[1]	0.002
HFA 227ea[1]	<0.001
HFA 134a - 10% (w/w) Ethanol[2]	0.014
HFA 227ea - 10% (w/w) Ethanol[2]	0.011

[1]From Williams (42).
[2]From Gelotte and Shadeed (43).

Lange and Finlay (19) have previously raised the possibility that water molecules may be attracted towards surfactant molecules present at droplet surfaces, creating a barrier to propellant evaporation. Such a phenomenon was not observed for the propellant-ethanol-surfactant formulation studied. As discussed in Section 2.5, the vapor pressure of HFA propellants is sufficiently high to establish a convective motion of vapor and air, known as Stefan flow, away from droplet surfaces. Where such a flow is present, any attraction of water molecules to droplet surfaces is likely overcome. Stefan flow becomes negligible when the partial pressure of vapor, p_S, at the droplet surface is much less than the total gas pressure there, p_{atm}; that is, when $p_S/p_{atm} << 1$ (4). However, to evaluate the vapor pressure of propellant droplets, the wet-bulb temperature must first be established. MATLAB script files (see Appendix D) were written to carry out the analytic solution outlined by Finlay (4) for the wet-bulb temperatures of isolated, spherical HFA 134a and 227ea droplets, under the assumption that Stefan flow may not be neglected. These temperatures were then used to determine *a posteriori* the corresponding ratios of p_S/p_{atm} for HFA droplets in both room and body temperature air. As seen in Table 5.2, Stefan flow may not be neglected for either HFA 134a or 227ea; rather, convective motion away from droplet surfaces plays a significant role in the evaporation of these propellants. It is therefore likely that any attraction polar water molecules may have towards surfactants at droplet surfaces is overcome by this outward flow, thereby preventing the presence of water vapor from altering the rate of propellant evaporation.

It is important to note that commercial MDIs predominantly employ HFA 134a as propellant, while the single droplet experiments were carried out with HFA 227ea.

TABLE 5.2

WET-BULB TEMPERATURES AND VAPOR PRESSURES OF HFA PROPELLANTS

Substance	Ambient Temperature (° C)	Wet-Bulb Temperature (° C)	Vapor Pressure, p_S (kPa)	p_S/p_{atm}
HFA 134a	20	-64	13.9	0.14
HFA 134a	37	-62	15.7	0.16
HFA 227ea	20	-53	17.1	0.17
HFA 227ea	37	-51	18.8	0.19
water	20	4	0.81	0.008

The ambient vapor concentration is assumed zero in all cases.
Values for water are given for comparison.

Unfortunately, HFA 134a's colder boiling point and higher vapor pressure (at a given temperature), as compared to HFA 227ea, make pendant droplet methods particularly difficult. Attempts to repeat the present study with HFA 134a as the propellant were not successful using the existing experimental apparatus and frame capture hardware. However, the arguments made above, along with data from Tables 5.1 and 5.2, do not suggest that HFA 134a will respond any differently than HFA 227ea to the presence of ambient water vapor. Based on the null result obtained from the experiments involving HFA 227ea (i.e. no difference in evaporation rates between dry and humid conditions), the decision was made not to invest the additional time and expenses necessary to adapt the experimental procedure in order to repeat the experiments using HFA 134a.

Referring again to the data collected for evaporation of HFA 227ea formulations, it may initially appear erroneous that no significant difference was observed between the evaporation rates of the pure propellant and the propellant-ethanol formulations. Ideally, the vapor pressure, and hence the evaporation rate, of a mixture of two liquids will

decrease linearly as the mole fraction of the less volatile component is increased, according to Raoult's Law. Therefore, with the addition of 15% (w/w) ethanol to the propellant, a reduction in the rate of evaporation would be expected. However, HFA-ethanol mixtures have been observed to exhibit a positive deviation from Raoult's Law, whereby the vapor pressure of the mixture remains constant despite the addition of appreciable fractions of ethanol (44, 45, 46). Vervaet and Byron (44) found that the vapor pressure of HFA 227ea-ethanol mixtures at room temperature remained fairly constant despite the addition of mole fractions of ethanol ranging from zero to approximately 0.5. The 15% (w/w) ethanol in HFA 227ea formulation studied in the present experiments has a mole fraction of ethanol of 0.4. Therefore, the similar evaporation rates observed for pure HFA 227ea and HFA 227ea-ethanol formulations may be explained by a positive deviation from Raoult's Law for the propellant-ethanol mixture.

Unlike the droplets studied here, which remained in contact with a column of the propellant-ethanol mixture held in the needle and syringe, droplets emitted from an MDI move freely through air. Therefore, the fraction of ethanol contained in MDI droplets is expected to increase as evaporation progresses, since the more volatile propellant evaporates at a much faster rate than the ethanol itself. At some time during the evaporation process, this increasing fraction of ethanol *will* affect the droplet vapor pressure. This is an important point to make. Smyth et al. (46) have stated that up to 20% ethanol may be added to HFA 134a formulations without significant increases in droplet size. However, their size measurements were made (by laser diffraction) only 6 cm from the MDI nozzle. In contrast, Gupta et al. (36) measured a decrease in fine

particle fraction from over 50% to approximately 25% as the ethanol concentration in HFA 134a MDI formulations was increased from 5% to 20% (w/w). Their size measurements were performed with an Aerodynamic Particle Sizer, separated from the USP 'throat' into which the MDIs were actuated by a 20 cm extension. It is therefore likely that Smyth et al. saw no changes in the aerosol size distribution of HFA 134a-ethanol MDIs only because they made size measurements at a point before any changes occurred. Indeed, in a later publication, Smyth is clear that even small concentrations of ethanol in HFA formulations can significantly affect aerosol size distributions (47). The point at which size measurements are made is clearly important, a detail that highlights the dynamic, time dependant nature of MDI aerosols.

5.2 Holding Chamber Bench Tests

When commercial MDIs were actuated into a mechanical ventilation holding chamber (Aerochamber®), increased holding chamber deposition and increased MMAD were observed in humid, as compared to dry, airflow. The two results go hand in hand, as it is well known that a particle's probability for inertial impaction increases monotonically with its Stokes number, which in turn is directly proportional to the particle diameter squared. In addition, a consistently larger holding chamber deposition was observed (in both dry *and* humid conditions) for the Ventolin® HFA formulation than for the Airomir® formulation, with no corroborating difference in the particle size distributions from the two MDIs. In this case, the increased deposition can be attributed to the visibly higher velocity of the aerosol cloud emitted from the MDI containing the Ventolin® HFA formulation. Particles traveling at a higher initial velocity will carry increased

momentum and be more likely to deposit in the holding chamber by impaction. Differences in the velocity of the aerosol cloud exiting MDI canisters of different manufacturers are common, and have been previously reported, for example by Barry and O'Callaghan (48).

Of greater interest to the present thesis is the fact that MMAD and holding chamber deposition increased significantly for both formulations, that is, regardless of the presence of cosolvent and surfactant (recall that the Ventolin® HFA formulation contains no excipients, while the Airmoir® formulation contains both cosolvent and surfactant). This result contradicts the hypothesis that interactions between surfactant and airborne water molecules, blocking evaporation of propellant at droplet surfaces, provide the primary mechanism through which deposition in the holding chamber increases with humidity. As argued in the previous section (Section 5.1), it is doubtful that the presence of ambient water vapor will have any effect on evaporation from a surface of pure propellant, like that of a Ventolin® HFA droplet. It is concluded that the observed increases in holding chamber deposition and particle size in humid airflow should not be attributed to a decreased rate of propellant evaporation from MDI droplets.

A widespread, competing explanation for the poor performance of MDIs exposed to high levels of ambient water vapor invokes the hypothesis that immediately following evaporation of the propellant, moisture condenses on the surfaces of cold residual drug particles, causing them to grow. Researchers have in the past dismissed this hypothesis after comparing MDI particle size measurements in dry versus humid conditions. Kim et al. (49) measured similar particle size distributions in dry and humid (90% RH) air at room temperature for a variety of drugs delivered by MDI, concluding that hygroscopic

growth of the particles was of no practical significance. Similarly, Lange and Finlay (19) measured nearly constant size distribution between dry and humid conditions for MDI particles delivered through a pediatric ventilator model, despite observing increased holding chamber deposition for the humid condition. At first glance, these results appear at odds with data from the present bench tests, in which MMAD was seen to increase dramatically between dry and humid conditions. However, for humid airflow, in the present tests MMAD later decreased as the distance between the holding chamber and cascade impactor was increased from 15 cm to 45 cm. For the constant flow rate of 28.3 l/min used in the bench tests, this increase in distance translates to an increase in the particles' travel time of approximately 200 msec. In contrast, Kim et al. actuated their MDIs into a 5 gallon (18.9 l) chamber, from which particles were drawn into a cascade impactor at a sampling flow rate of 28 l/min. With such an experimental design, MDI particles might remain in the chamber for well over 30 seconds, allowing ample time for any transient increase in particle sizes to reverse. In their model of a pediatric ventilator circuit, Lange and Finlay set an inhalation flow rate of 4.8 l/min through a holding chamber identical to that used in the present study. On average, MDI particles would have remained in the holding chamber six times longer in Lange and Finlay's study than in the present bench tests. In addition, due to the small tidal volume of the pediatric model, the holding chamber would not have been completely cleared in a single tidal breath, increasing the time between MDI actuation and particle sampling even further for those particles suspended in the holding chamber between breaths. It is conceivable that moisture, having condensed on cold MDI particles during an initial transient period, had

re-evaporated into the ambient flow of air prior to particle sampling, thus resulting in a measured particle size distribution identical to that recorded for dry airflow.

To obtain an understanding of how such a sequence of particle growth followed by evaporation might occur, it is instructive to consider Equation 2.12, which governs the temperature of a droplet under the assumptions of simplified hygroscopic theory.

$$-LD(c_S - c_\infty) - k_{air}(T - T_\infty) = \frac{dT}{dt}\rho c_P \frac{d^2}{12} \tag{2.12}$$

where L — latent heat of vaporization;
D — diffusion coefficient of droplet vapor in air;
c_S, c_∞ — vapor concentrations at, and far away from, droplet surface.
k_{air} — thermal conductivity of air;
T_∞ — ambient temperature far from the droplet;
T — droplet temperature;
c_P — specific heat capacity of the droplet;
d — droplet diameter;
t — time.

It is known that a droplet introduced to a new ambient environment will quickly adjust to a constant, 'wet-bulb' temperature, which can be determined for a given ambient temperature and relative humidity by setting the right hand side of Equation (2.12) to zero. However, a transient period must exist in which the droplet temperature adjusts from its initial value to its wet-bulb value. During propellant evaporation, a suspended MDI particle will be cooled to very low temperature. In addition, propellant evaporation will locally cool the humid air surrounding MDI particles, causing it to become supersaturated with water vapor. Therefore, immediately following complete evaporation of the propellant, the cold, residual drug particles likely act as condensation

nuclei, causing a layer of water molecules to adsorb to each particle surface. Provided the drug does not dissolve into the adsorbed water, an assumption that will be discussed below, the MDI particles will then behave in identical fashion to water droplets of the same size (29).

Energy transferred to the newly formed droplets through continued condensation, and through conduction of heat from the much warmer ambient air, will quickly raise the droplet temperatures to their constant, wet-bulb value. The wet-bulb temperature of the droplets may be calculated by setting the right hand side of Equation 2.12 to zero. Figure 5.1 displays calculated wet-bulb temperatures for water droplets in 37° C, nearly saturated air, typical of the conditions found in a ventilator circuit. Droplet temperature is predicted to be lower than that of the ambient air so long as the concentration of water

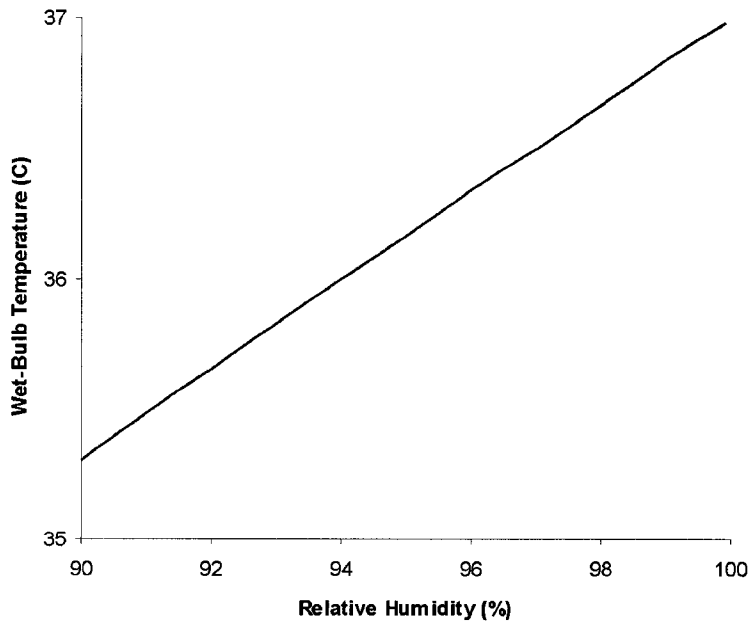

Figure 5.1 Wet-bulb temperatures for water droplets in 37° C air.

vapor is below saturation (i.e. RH < 100%). In such a case, in order to maintain the constant wet-bulb temperature, heat transferred to a droplet must be balanced by an energy loss due to evaporation. That is to say, after an initial period of temperature adjustment, water droplets are expected to evaporate even in highly humid air, so long as the concentration of water vapor in air is below saturation. Consideration of the three terms in Equation 2.12 during this process is made in Table 5.3.

TABLE 5.3

MASS (OF WATER) AND HEAT TRANSFER FOR MDI PARTICLES IN BELOW-SATURATED HUMID AIR

Timeline	$c_S - c_\infty$*	$T - T_\infty$	dT/dt
Transient growth	< 0	< 0	> 0
Maximum Size	$= 0$	< 0	> 0
Steady-state evaporation	> 0	< 0	$= 0$

* For c_∞ below saturation, $c_\infty = n\, c_{Saturation}(T_\infty)$, where $n < 1$.

5.3 Future Work

Based on the above analysis, a three-step sequence is proposed to explain the size changes undergone by MDI droplets released into humid airflow:

1.) Rapid, unobstructed evaporation of propellant from non-volatile components in the MDI formulation (i.e. drug, surfactant).

2.) Transient growth of propellant-cooled, non-volatile particles due to condensation of water.

3.) Steady state evaporation of water from non-volatile particles.

The presence of non-volatile surfactant molecules in the MDI formulation may reduce the rate of mass transfer of water to or from particle surfaces by several orders of magnitude through formation of surface films, or monolayers (50, 51). In the present bench tests, no such dramatic difference was observed in the rate of change of particle size downstream from the holding chamber between the Airomir® formulation (which contained oleic acid surfactant) and the Ventolin® HFA formulation (which was surfactant-free). The surfactant in the Airomir® formulation likely did not entirely coat the MDI particles, so that its effect was diminished (52). The possibility that surfactant molecules added to the MDI formulation might be employed to reduce particle growth in humid airflow remains to be studied.

In addition to the effect of surfactants, the solubility of the drug itself in the condensed water will affect further mass transfer by reducing the vapor pressure of the water (4, 24). Such a reduction in vapor pressure would be expected to enhance condensation, and retard evaporation, of water at particle surfaces. As both MDIs studied in the bench tests delivered salbutamol sulphate, the relative influence of different drugs on particle size changes was not evaluated.

As discussed in the previous section, given sufficient time, steady state evaporation of water from MDI particles may largely negate the initial nucleated condensation. It is therefore possible that losses in the ventilator circuit can be diminished through the use of a large-volume holding chamber. Indeed, Lange and Finlay (19) have shown that for their *in vitro* model of a pediatric ventilator circuit, deposition in a large, prototypical chamber is not increased in humid airflow. As the volume of this chamber is approximately 30 times larger than that of a single tidal breath

(in the pediatric model), the size of the chamber allows MDI particles to ample time to undergo size changes while suspended between breaths. It remains to be seen if practical size limitations make large-volume chambers unfeasible for ventilation of adults, where tidal volumes are an order of magnitude greater than those for children. Optimization of the size of mechanical ventilation holding chambers, for both pediatric and adult use, is a subject for future work.

Chapter 6

Summary

The goal of the present work was to determine the primary mechanism by which delivery of drug to the lung is reduced when MDIs are actuated into the warm, humid airflow supplied during mechanical ventilation of intubated patients. Although previous authors have proposed a variety of manners in which increased concentrations of ambient water vapor may negatively affect delivery of MDI aerosols, the majority (and most plausible) of explanations can be divided into two groups. The first blames aerosol losses in the ventilator circuit on increased particle sizes as a result of a retarded rate of propellant evaporation from MDI particles in the presence of high humidity. The second suggests that it is condensation of water on MDI particles that leads to increased sizes, thereby augmenting aerosol deposition in the ventilator circuit. In the work leading to this thesis, experiments were performed to evaluate the likelihood that either of these two mechanisms is responsible for the adverse effect of humidity on MDI drug delivery.

Single, pendant droplet experiments were used to investigate the effects of humidity and MDI formulation on evaporation of HFA 227ea propellant. No significant difference in the rate of evaporation was observed between dry and humid conditions for formulations of pure propellant; propellant and 15% (w/w) ethanol; or propellant, 15% ethanol, and 0.2% sorbitan trioleate. These experimental results were supported by theoretical arguments against any effect of water vapor at a propellant-air interface, based

on the lack of strong intermolecular attractions between water and HFA propellants, and the presence of Stefan flow of the gaseous phase away from the interface.

A second study was performed to investigate the effect of humidity on holding chamber deposition and particle size distributions from two commercial salbutamol sulphate MDIs. While the Airomir® formulation contained both ethanol cosolvent and oleic acid surfactant, the Ventolin® HFA formulation contained no excipients. Deposition in the holding chamber was observed to increase between dry and humid conditions for either MDI, that is, regardless of the presence of excipients in the formulation. In addition, similar increases in particle size in the presence of humidity were measured downstream from the holding chamber for the two formulations. For the formulations studied, added excipients did not play a major role in determining the observed increases in particle size in humid airflow.

The evolution of particle sizes downstream from the holding chamber was determined by taking a second set of size measurements, with the distance between the holding chamber and cascade impactor increased from 15 cm to 45 cm. For dry conditions, no significant change to the particle size distribution from either MDI was observed, implying that the particles had reached their final sizes prior to the measurement at 15 cm. However, for the humid case, the MMAD of the aerosol from either MDI was observed to decrease significantly, while the GSD increased significantly, between the 15 cm and 45 cm measurements. This data indicated that MDI particles, which had increased in size in the presence of high concentrations of ambient water vapor, were decreasing in size downstream from the holding chamber.

Based on consideration of the energy transfer to and from MDI particles as they change size, a three step process was proposed to explain the progression of size changes undergone by MDI aerosols emitted into confined, humid settings, as found during mechanical ventilation. First, the propellant rapidly evaporates from non-volatile components in the MDI formulation (i.e. drug, surfactant), without obstruction. Immediately following propellant evaporation, ambient water adsorbs to particle surfaces, initiating a transient growth of propellant-cooled, non-volatile particles due to further condensation of water. Finally, in the steady state, the newly formed water droplets may evaporate back into the ambient air.

Subjects that were identified for future work include the affects of non-volatile surfactants, and of dissolution of drug, on hygroscopic size changes of MDI particles. In addition, the use of large-volume holding chambers was noted as a possible means of circumventing aerosol deposition in ventilator circuits. Optimization of the size of prototypical holding chambers is required to determine whether practical size limitations preclude the use of such chambers in clinical settings.

In conclusion, this work has provided new evidence to refute some common explanations of the poor performance of MDIs in humid settings. A process has been proposed, for the first time, to link the hypothesis of condensative particle growth with the size data reported in this work, and by previous authors.

References

1. Grossman J. 1994. The evolution of inhaler technology. *J. of Asthma.* 31(1): 55-64.

2. O'Callaghan C, Nerbink O, and MT Vidgren. 2002. The history of inhaled drug delivery. In: Bisgaard H, O'Callaghan C, and GC Smaldone (eds.). *Drug Delivery to the Lung.* Marcel Dekker, New York.

3. Smaldone GC, and PN LeSouef. 2002. Nebulization: the device and clinical considerations. In: Bisgaard H, O'Callaghan C, and GC Smaldone (eds.). *Drug Delivery to the Lung.* Marcel Dekker, New York.

4. Finlay WH. 2001. *The Mechanics of Inhaled Pharmaceutical Aerosols: An Introduction.* Academic Press, London.

5. Patridge MR, and AA Woodcock. 2002. Propellants. In: Bisgaard H, O'Callaghan C, and GC Smaldone (eds.). *Drug Delivery to the Lung.* Marcel Dekker, New York.

6. Wright P. 2002. Environmental regulation and HFA metered-dose inhalers: perspectives from the pharmaceutical industry. In: Dalby RN, Byron PR, Peart J, and SJ Farr (eds.). *Respiratory Drug Delivery VIII.* Virginia Commonwealth University, Richmond, VA.

7. Jashnani R, Byron P, and R Dalby. 1995. Testing of dry powder aerosol formulations in different environmental conditions. *Int J Pharm.* 113: 123-130.

8. Dunbar CA, Hickey AJ, and P Holzner. 1998. Dispersion and characterization of pharmaceutical dry powder aerosols. *KONA, Powder and Particle.* 16: 7-45.

9. Borgstom L, Bisgaard H, O'Callaghan C, and S Pedersen. 2002. Dry-powder inhalers. In: Bisgaard H, O'Callaghan C, and GC Smaldone (eds.). *Drug Delivery to the Lung.* Marcel Dekker, New York.

10. Gammon RB, Strickland JH, Kennedy JI, and KR Young. 1995. Mechanical ventilation – a review for the internist. *Am. J. Med.* 99(5): 553-562.

11. Esteban A, Anuzueto A, Alia I, Gordo F, Apezteguia C, Palizas F, Cide D, Goldwaser R, Soto L, Bugedo G, Rodrigo C, Pimentel J, Raimondi G, and MJ Tobin. 2000. How is mechanical ventilation employed in the intensive care unit? An international utilization review. *Am. J. Respir. Crit. Care Med.* 161(5): 1450-1458.

12. Estes R, and G Meduri. 1995. The pathogenesis of ventilator-associated pneumonia; 1, mechanics of bacterial transcolonization and airway inoculation. *Int. Care Med.* 21: 365-383.

13. Georgopolous D, Mouloudi E, Kondili E, and M Klimathianaki. 2000. Bronchodilator delivery with metered-dose inhaler during mechanical ventilation. *Crit. Care*. 4(4): 227-234.

14. Dhand R, and MJ Tobin. 1996. Bronchodilator delivery with metered-dose inhalers in mechanically-ventilated patients. *Eur. Respir. J.* 9: 585-595.

15. Georgopolous D, and H Burchardi. 1998. Ventilatory strategies in adult patients with status asthmaticus. *Eur Respir Monit.* 8: 45-83.

16. Hess D. 2002. Aerosol delivery during mechanical ventilation. *Minerva Anestesiologica.* 65(5): 321-325.

17. Diot P, Morra L, and GC Smaldone. 1995. Albuterol delivery in a model of mechanical ventilation: comparison of metered-dose inhaler and nebulizer efficiency. *Am. J. Respir. Crit. Care Med.* 152: 1391-1394.

18. Fink JB, Dhand R, Duarte AG, Jenne JW, and MJ Tobin. 1996. Aerosol delivery from a metered-dose inhaler during mechanical ventilation. *Am. J. Respir. Crit. Care Med.* 154: 382-387.

19. Lange CF, and WH Finlay. 2000. Overcoming the adverse effect of humidity in aerosol delivery via pressurized metered-dose inhalers during mechanical ventilation. *Am. J. Respir. Crit. Care Med.* 161: 1614-1618.

20. Wildhaber JH, Hayden MJ, Dore ND, Devadason SG, and PN LeSouef. 1998. Salbutamol delivery from a hydrofluoroalkane pressurized metered-dose inhaler in pediatric ventilator circuits. *Chest.* 113:186-191.

21. Garner SS, Wiest DB, Bradley JW, Lesher BA, and DM Habib. 1996. Albuterol delivery by metered-dose inhaler in a mechanically ventilated pediatric model. *Crit. Care Med.* 24: 870-874.

22. Fink JB, Dhand R, Grychowski J, Fahey PJ, and MJ Tobin. 1999. Reconciling *in vitro* and *in vivo* measurements of aerosol delivery from a metered-dose inhaler during mechanical ventilation and defining efficiency-enhancing factors. *Am. J. Respir. Crit. Care Med.* 159: 63-68.

23. Baron PA, and K Willeke (eds.). 1993. *Aerosol Measurement.* Van Nostrand Reinhold, New York.

24. Hinds WC. 1999. *Aerosol Technology.* John Wiley & Sons, New York.

25. Finlay WH, DeHaan W, Grgic B, Heenan A, Matida EA, Hoskinson M, Pollard A, and CF Lange. 2002. Fluid mechanics and particle deposition in the oropharynx: the factors that really matter. In: RN Dalby, PR Byron, J Peart, and SJ Farr (eds.). *Respiratory Drug Delivery VIII.* Virginia Commonwealth University, Richmond, VA.

26. DeHaan WH, and WH Finlay. 2004. Predicting extrathoracic deposition from dry powder inhalers. *J. Aerosol Sci.* 35: 309-331.

27. Ingham DB. 1975. Diffusion of aerosols from a stream flowing through a cylindrical tube. *J. Aerosol Sci.* 6: 125-132.

28. Gormley PG, and K Kennedy. 1949. Diffusion from a stream flowing through a cylindrical tube. *Proc. Roy. Irish Soc.* 52A: 163.

29. Crampton M, Kinnersley R, and J Ayres. Sub-micrometer particle production by pressurized metered dose inhalers. *J. Aerosol Med.* 17(1): 33-42.

30. Fuchs NA. 1959. *Evaporation and Droplet Growth in Gaseous Media.* Pergamon Press, Oxford.

31. Maxwell JC. 1890. *The Scientific Papers of James Clerk Maxwell.* Cambridge University Press, Cambridge.

32. Sirignano WA. 1993. Fluid dynamics of sprays – 1992 Freeman Scholar Lecture. *J. Fluids Eng.* 115:345-378.

33. Clark AR. 1991. Metered atomization for respiratory drug delivery. Ph.D. thesis, Loughborough University of Technology, U.K.

34. Dunbar CA, Watkins AP, and JF Miller. 1997. Theoretical investigation of the spray from a pressurized metered-dose inhaler. *Atomization and Sprays.* 7: 417-436.

35. Hickey AJ, and RM Evans. 1996. Aerosol generation from propellant-driven metered dose inhalers. In *Inhalation Aerosols: Physical and Biological Basis for Therapy.* AJ Hickey (ed.), Marcel Dekker, New York, pp. 417-439.

36. Gupta A, Stein SW, and PB Myrdal. 2003. Balancing ethanol cosolvent concentration with product performance in 134a-based pressurized metered dose inhalers. *J. Aerosol Med.* 16(2): 167-174.

37. Lin JC, and JW Gentry. 2003. Spray drying drop morphology: experimental study. *Aerosol Sci. Tech.* 37: 15-32.

38. Lahooti S, Del Rio OI, Neumann AW, and P Cheng. 1996. Axisymmetric drop shape analysis (ADSA). In: *Applied Surface Thermodynamics*. Marcel Dekker, New York.

39. Cheng P. 1990. Automation of axisymmetric drop shape analysis using digital image processing. Ph.D. Thesis, University of Toronto, Toronto.

40. Press WH, Teukolsky SA, Vetterling WT, and BP Flannery. 2002. *Numerical Recipes in C++ (2nd edition)*, Cambridge University Press, Cambridge.

41. Finlay WH, and KW Stapleton. 1999. Undersizing of droplets from a vented nebulizer caused by aerosol heating during transit through an Andersen impactor. *J. Aerosol Sci.* 30(1): 105-109.

42. Williams G. 1999. Moisture transport into CFC-free MDIs. *J. Allergy Clin. Immun.* 104 (6): S227-S229.

43. Gelotte KM, and DJ Shadeed. 1998. Water solubility in metered-dose inhalers media containing different propellants. *Pharm. Sci.* 1: 210.

44. Vervaet C, and PR Byron. 1999. Drug-surfactant-propellant interactions in HFA-formulations. *Int. J. Pharm.* 186:13-30.

45. Tzou TZ. 1998. Density, excess molar volume, and vapor pressure of propellant mixtures in metered-dose inhalers: deviation from ideal mixtures. In: Byron PR, Dalby RN, and SJ Farr (eds.). *Respiratory Drug Delivery VI.* Interpharm Press, Buffalo Grove, IL.

46. Smyth HDC, Mejia-Millan EA, and AJ Hickey. 2002. The effect of ethanol on solvency, vapor pressure, and emitted droplet size of solution metered dose inhalers containing HFA 134a. In: RN Dalby, PR Byron, J Peart, and SJ Farr (eds.). *Respiratory Drug Delivery VIII.* Virginia Commonwealth University, Richmond, VA.

47. Smyth HDC. 2003. The influence of formulation variables on the performance of alternative propellant-driven metered dose inhalers. *Adv. Drug Del. Rev.* 55: 807-828.

48. Barry PW, and C O'Callaghan. 1997. *In vitro* comparison of the amount of salbutamol available for inhalation from different formulations used with different spacer devices. *Eur. Respir. J.* 10: 1345-1348.

49. Kim CS, Trujillo D, and MA Sacker. 1985. Size aspects of metered-dose inhaler aerosols. *Am. Rev. Respir. Dis.* 132: 137-142.

50. Barnes GT. 1986. The effects of monolayers on the evaporation of liquids. *Adv. Colloid Interface Sci.* 25: 89-200.

51. Otani Y, and CS Wang. 1984. Growth and deposition of saline droplets covered with a monolayer of surfactant. *Aerosol. Sci. Tech.* 3: 155-166.

52. Derjaguin BV, Fedoseyev VA, and LA Rosenzweig. 1966. Investigation of the adsorption of cetyl alcohol vapor and the effect of this phenomenon on the evaporation of water drops. *J. Colloid Interface Sci.* 22: 45-50.

Appendix A

Pendant Droplet Data

HFA 227ea; 37° C, < 10% RH

Droplet 1:

Time (s)	Droplet Volume (ml)
0	0.003895046
0.143	0.003320548
0.358	0.002587411
0.521	0.002236408
0.631	0.001879631
0.806	0.001254568
0.931	0.001073812

Slope = -0.0030 ml/s; $R^2 = 0.993$

Droplet 2:

Time (s)	Droplet Volume (ml)
0	0.004087564
0.232	0.003258741
0.376	0.002156821
0.535	0.002098632
0.796	0.001214876
0.952	0.000896311

Slope = -0.0033 ml/s; $R^2 = 0.956$

Droplet 3:

Time (s)	Droplet Volume (ml)
0	0.003795181
0.171	0.003157251
0.401	0.002458762
0.527	0.002351875
0.702	0.001457821
0.831	0.001136841
1.069	0.001124876

Slope = -0.0027 ml/s; $R^2 = 0.947$

Droplet 4:

Time (s)	Droplet Volume (ml)
0	0.003895045
0.126	0.003150875
0.361	0.002681542
0.470	0.002048399
0.591	0.001899651
0.805	0.001341157
0.950	0.001050893

Slope = -0.0029 ml/s; $R^2 = 0.973$

Droplet 5:

Time (s)	Droplet Volume (ml)
0	0.003581084
0.170	0.003369817
0.363	0.002251835
0.490	0.002038451
0.699	0.001458739
0.840	0.001154892
0.985	0.001082870

Slope = -0.0028 ml/s; $R^2 = 0.953$

Droplet 6:

Time (s)	Droplet Volume (ml)
0	0.004021575
0.223	0.003268742
0.433	0.002781192
0.562	0.002238189
0.684	0.001411584
0.909	0.001126728
1.135	0.001128705

Slope = -0.0028 ml/s; $R^2 = 0.926$

Droplet 7:

Time (s)	Droplet Volume (ml)
0	0.003751943
0.125	0.003387281
0.265	0.003014725
0.450	0.002438943
0.654	0.001750876
0.898	0.001240846
1.060	0.001113588

Slope = -0.0026 ml/s; $R^2 = 0.983$

Droplet 8:

Time (s)	Droplet Volume (ml)
0	0.004128456
0.175	0.004287024
0.386	0.003284054
0.572	0.002872801
0.725	0.002262480
0.920	0.001847205
1.072	0.001124804
1.293	0.001027899

Slope = -0.0028 ml/s; $R^2 = 0.967$

Droplet 9:

Time (s)	Droplet Volume (ml)
0	0.003540876
0.127	0.003365484
0.328	0.002400578
0.490	0.002257305
0.649	0.001862048
0.898	0.001421381
1.090	0.001145762

Slope = -0.0022 ml/s; $R^2 = 0.962$

Droplet 10:

Time (s)	Droplet Volume (ml)
0	0.003302784
0.276	0.002872025
0.475	0.002150487
0.743	0.001354042
0.913	0.001024584
1.167	0.000847505

Slope = -0.0023 ml/s; $R^2 = 0.964$

Droplet 11:

Time (s)	Droplet Volume (ml)
0	0.003890547
0.150	0.003524581
0.338	0.002735056
0.561	0.002214896
0.783	0.002183084
0.898	0.001248435
1.141	0.000946827

Slope = -0.0026 ml/s; $R^2 = 0.958$

Droplet 12:

Time (s)	Droplet Volume (ml)
0	0.003468127
0.208	0.002982741
0.338	0.002867024
0.549	0.002248734
0.900	0.001428043
1.008	0.001402784
1.160	0.001028494

Slope = -0.0021 ml/s; $R^2 = 0.992$

Droplet 13:

Time (s)	Droplet Volume (ml)
0	0.003570247
0.225	0.003105738
0.394	0.002758025
0.633	0.002347197
0.716	0.002105687
0.816	0.002127902
0.953	0.001325078
1.185	0.001248045

Slope = -0.0020 ml/s; $R^2 = 0.967$

Droplet 14:

Time (s)	Droplet Volume (ml)
0	0.003450548
0.212	0.002784057
0.468	0.002680248
0.646	0.002223818
0.830	0.001519379
0.971	0.001148753
1.144	0.001035754

Slope = -0.0022 ml/s; $R^2 = 0.962$

Droplet 15:

Time (s)	Droplet Volume (ml)
0	0.003170157
0.117	0.002404876
0.359	0.002279241
0.574	0.001769143
0.719	0.001225874
0.925	0.001104387

Slope = -0.0021 ml/s; $R^2 = 0.935$

Droplet 16:

Time (s)	Droplet Volume (ml)
0	0.003514846
0.167	0.003240275
0.414	0.002387046
0.580	0.001724928
0.753	0.001324873
0.886	0.001120457

Slope = -0.0029 ml/s; $R^2 = 0.986$

Droplet 17:

Time (s)	Droplet Volume (ml)
0	0.004350457
0.161	0.003958712
0.323	0.002820246
0.550	0.002314315
0.800	0.001474859
0.992	0.001240575
1.167	0.001198201

Slope = -0.0029 ml/s; $R^2 = 0.936$

Droplet 18:

Time (s)	Droplet Volume (ml)
0	0.004608751
0.243	0.004022974
0.461	0.003468187
0.707	0.002340577
0.897	0.001858748
1.096	0.001568724
1.243	0.001014824

Slope = -0.0030 ml/s; $R^2 = 0.988$

Droplet 19:

Time (s)	Droplet Volume (ml)
0	0.004258405
0.173	0.003754388
0.430	0.002895024
0.613	0.002611284
0.842	0.001751058
1.054	0.001429878
1.171	0.001223648

Slope = -0.0026 ml/s; R^2 = 0.989

Droplet 20:

Time (s)	Droplet Volume (ml)
0	0.003782046
0.183	0.003256841
0.397	0.002578180
0.538	0.001987512
0.743	0.001758894
0.882	0.001366940
1.063	0.001241138

Slope = -0.0025 ml/s; R^2 = 0.965

Summary:

Number of droplets = 20
Mean slope = 2.62 ± 0.36 µl/s

HFA 227ea; 37° C, 100% RH

Droplet 1:

Time (s)	Droplet Volume (ml)
0	0.003982045
0.232	0.003722612
0.372	0.003682015
0.585	0.002982418
0.910	0.001348722
1.034	0.001173182

Slope = -0.0030 ml/s; R^2 = 0.928

Droplet 2:

Time (s)	Droplet Volume (ml)
0	0.004028793
0.208	0.003428197
0.389	0.003266087
0.507	0.002781376
0.744	0.001832057
0.925	0.001255684
1.089	0.001058738

Slope = -0.0029 ml/s; R^2 = 0.979

Droplet 3:

Time (s)	Droplet Volume (ml)
0	0.003581204
0.172	0.003228705
0.312	0.002691755
0.423	0.002588933
0.581	0.002218077
0.833	0.001425587
0.989	0.001204385

Slope = -0.0025 ml/s; R^2 = 0.991

Droplet 4:

Time (s)	Droplet Volume (ml)
0	0.003281702
0.108	0.003215785
0.324	0.002591873
0.467	0.002266982
0.695	0.001627084
0.878	0.001105789

Slope = -0.0026 ml/s; $R^2 = 0.992$

Droplet 5:

Time (s)	Droplet Volume (ml)
0	0.003894205
0.187	0.003754805
0.290	0.003261054
0.391	0.002885023
0.568	0.002058482
0.801	0.001869374
0.998	0.001582614
1.139	0.000985127

Slope = -0.0026 ml/s; $R^2 = 0.960$

Droplet 6:

Time (s)	Droplet Volume (ml)
0	0.003528431
0.107	0.003368221
0.299	0.002505408
0.406	0.002216635
0.656	0.001759054
0.787	0.001563054
0.996	0.001136481

Slope = -0.0024 ml/s; $R^2 = 0.967$

Droplet 7:

Time (s)	Droplet Volume (ml)
0	0.003896032
0.196	0.003580421
0.426	0.003362581
0.702	0.002460238
0.784	0.001893024
0.999	0.001560247
1.180	0.001205766

Slope = -0.0024 ml/s; $R^2 = 0.967$

Droplet 8:

Time (s)	Droplet Volume (ml)
0	0.003963805
0.151	0.003581243
0.401	0.003225894
0.528	0.002690842
0.748	0.002105548
0.870	0.001896632
1.111	0.001325782
1.338	0.001028435

Slope = -0.0023 ml/s; $R^2 = 0.989$

Droplet 9:

Time (s)	Droplet Volume (ml)
0	0.003687281
0.223	0.003268850
0.430	0.003058124
0.585	0.002655381
0.751	0.002258045
0.900	0.001583197
0.990	0.001548765
1.210	0.001125871
1.404	0.001028549

Slope = -0.0021 ml/s; $R^2 = 0.971$

Droplet 10:

Time (s)	Droplet Volume (ml)
0	0.004057832
0.171	0.003687251
0.373	0.002563785
0.477	0.002227539
0.714	0.001634725
0.926	0.001385244
1.144	0.001035874
1.341	0.001018842

Slope = -0.0024 ml/s; $R^2 = 0.910$

Droplet 11:

Time (s)	Droplet Volume (ml)
0	0.003580543
0.181	0.002498322
0.287	0.001768971
0.497	0.001206975
0.742	0.001182234

Slope = -0.0032 ml/s; $R^2 = 0.830$

Droplet 12:

Time (s)	Droplet Volume (ml)
0	0.003420579
0.141	0.003029855
0.370	0.002469182
0.474	0.001983268
0.594	0.001351894
0.631	0.001102584

Slope = -0.0036 ml/s; $R^2 = 0.968$

Droplet 13:

Time (s)	Droplet Volume (ml)
0	0.003682284
0.210	0.003124979
0.434	0.002580527
0.630	0.002048332
0.740	0.001581837
0.975	0.001200688

Slope = -0.0026 ml/s; $R^2 = 0.993$

Droplet 14:

Time (s)	Droplet Volume (ml)
0	0.003458025
0.127	0.003158890
0.348	0.002693911
0.460	0.002450258
0.607	0.001837785
0.727	0.001405268
0.969	0.001034825

Slope = -0.0026 ml/s; $R^2 = 0.983$

Droplet 15:

Time (s)	Droplet Volume (ml)
0	0.003350877
0.173	0.003159378
0.310	0.002205874
0.549	0.002125824
0.829	0.001405988
0.965	0.001139259
1.107	0.000931587

Slope = -0.0022 ml/s; $R^2 = 0.956$

Droplet 16:

Time (s)	Droplet Volume (ml)
0	0.003705781
0.194	0.003389157
0.439	0.002405381
0.641	0.001795324
0.782	0.001322557
1.015	0.001191379

Slope = -0.0028 ml/s; $R^2 = 0.963$

Droplet 17:

Time (s)	Droplet Volume (ml)
0	0.004028186
0.159	0.003789245
0.409	0.002628157
0.548	0.002512057
0.699	0.001683781
0.910	0.001254986
1.121	0.001058433

Slope = -0.0029 ml/s; $R^2 = 0.964$

Droplet 18:

Time (s)	Droplet Volume (ml)
0	0.003892024
0.140	0.003682287
0.291	0.003128739
0.485	0.002548087
0.604	0.002239988
0.740	0.002139127
0.950	0.001450573
1.138	0.001103594

Slope = -0.0025 ml/s; $R^2 = 0.989$

Droplet 19:

Time (s)	Droplet Volume (ml)
0	0.003405781
0.196	0.003260548
0.341	0.002828973
0.470	0.002561918
0.704	0.001728731
0.896	0.001357199
1.100	0.001105488
1.360	0.001105384

Slope = -0.0020 ml/s; $R^2 = 0.938$

Droplet 20:

Time (s)	Droplet Volume (ml)
0	0.003587211
0.209	0.003295054
0.469	0.003098802
0.604	0.002218437
0.860	0.001799824
1.029	0.001302741
1.212	0.001318942
1.469	0.001124873

Slope = -0.0019 ml/s; $R^2 = 0.933$

Summary:

Number of droplets = 20
Mean slope = 2.58 ± 0.41 µl/s

HFA 227ea-EtOH(15% w/w); 37° C, < 10% RH

Droplet 1:

Time (s)	Droplet Volume (ml)
0	0.003868751
0.182	0.003680457
0.399	0.002450578
0.539	0.001637824
0.682	0.001322688
0.785	0.001112484

Slope = -0.0039 ml/s; R^2 = 0.963

Droplet 2:

Time (s)	Droplet Volume (ml)
0	0.004028437
0.162	0.003668272
0.292	0.003251978
0.534	0.002782057
0.665	0.002264378
0.795	0.001420568
0.971	0.001034873

Slope = -0.0031 ml/s; R^2 = 0.973

Droplet 3:

Time (s)	Droplet Volume (ml)
0	0.003780543
0.202	0.003102549
0.463	0.002527813
0.609	0.001633579
0.804	0.001257915
0.932	0.001022546

Slope = -0.0031 ml/s; R^2 = 0.980

Droplet 4:

Time (s)	Droplet Volume (ml)
0	0.004058137
0.105	0.003982406
0.230	0.003424028
0.391	0.002438870
0.538	0.001893705
0.760	0.001458921
0.990	0.001135781

Slope = -0.0033 ml/s; R^2 = 0.945

Droplet 5:

Time (s)	Droplet Volume (ml)
0	0.004281305
0.242	0.003890245
0.353	0.003369127
0.529	0.002528737
0.780	0.002105558
0.921	0.001678924
1.149	0.001240876
1.363	0.001157294

Slope = -0.0025 ml/s; R^2 = 0.958

Droplet 6:

Time (s)	Droplet Volume (ml)
0	0.003725408
0.232	0.003459122
0.352	0.002879124
0.485	0.002267504
0.636	0.001597024
0.826	0.001336728
1.045	0.001175844

Slope = -0.0028 ml/s; R^2 = 0.934

Droplet 7:

Time (s)	Droplet Volume (ml)
0	0.004089124
0.058	0.003805478
0.252	0.003362815
0.472	0.002824753
0.783	0.002314741
0.987	0.001452087
1.195	0.001024897

Slope = -0.0025 ml/s; $R^2 = 0.990$

Droplet 8:

Time (s)	Droplet Volume (ml)
0	0.003750432
0.218	0.003108755
0.398	0.002680248
0.511	0.002014742
0.743	0.001358025
0.987	0.001199752
1.178	0.001124687

Slope = -0.0024 ml/s; $R^2 = 0.925$

Droplet 9:

Time (s)	Droplet Volume (ml)
0	0.004205798
0.115	0.003780246
0.265	0.003363254
0.387	0.003102487
0.530	0.002757841
0.799	0.002225018
0.919	0.001657811
1.066	0.001345872
1.235	0.001120587

Slope = -0.0025 ml/s; $R^2 = 0.992$

Droplet 10:

Time (s)	Droplet Volume (ml)
0	0.004087925
0.156	0.003810573
0.372	0.003491738
0.566	0.003025789
0.804	0.002257905
1.029	0.001598224
1.278	0.001205782

Slope = -0.0024 ml/s; $R^2 = 0.987$

Droplet 11:

Time (s)	Droplet Volume (ml)
0	0.003705489
0.227	0.003362475
0.416	0.002650548
0.594	0.002491275
0.729	0.001763822
0.960	0.001325774
1.173	0.001024802

Slope = -0.0024 ml/s; $R^2 = 0.977$

Droplet 12:

Time (s)	Droplet Volume (ml)
0	0.003894028
0.211	0.003368424
0.422	0.002983457
0.562	0.002462057
0.774	0.002039675
1.015	0.001627742
1.187	0.001205732

Slope = -0.0023 ml/s; $R^2 = 0.994$

Droplet 13:

Time (s)	Droplet Volume (ml)
0	0.003680574
0.152	0.003362711
0.262	0.003028875
0.404	0.002439182
0.560	0.002368277
0.813	0.001328941
0.970	0.001165827
1.107	0.000982731

Slope = -0.0026 ml/s; R^2 = 0.980

Droplet 14:

Time (s)	Droplet Volume (ml)
0	0.003905721
0.117	0.003758886
0.267	0.003450278
0.394	0.003100572
0.621	0.002105789
0.883	0.001637854
1.105	0.001258137
1.238	0.001024873

Slope = -0.0025 ml/s; R^2 = 0.981

Droplet 15:

Time (s)	Droplet Volume (ml)
0	0.003780244
0.304	0.003028438
0.509	0.002459136
0.729	0.002231178
0.947	0.001860357
1.114	0.001420579
1.298	0.001123616

Slope = -0.0020 ml/s; R^2 = 0.988

Droplet 16:

Time (s)	Droplet Volume (ml)
0	0.003925105
0.241	0.003365281
0.404	0.002463872
0.614	0.001705724
0.728	0.001352288
0.811	0.000896721

Slope = -0.0038 ml/s; R^2 = 0.988

Droplet 17:

Time (s)	Droplet Volume (ml)
0	0.003872912
0.179	0.003682407
0.339	0.002841057
0.440	0.002435182
0.573	0.001983272
0.800	0.001420558
0.914	0.001134278

Slope = -0.0032 ml/s; R^2 = 0.979

Droplet 18:

Time (s)	Droplet Volume (ml)
0	0.003982054
0.232	0.003680277
0.352	0.002982739
0.554	0.002241873
0.770	0.001863721
0.967	0.001430279
1.126	0.001022473

Slope = -0.0027 ml/s; R^2 = 0.977

Droplet 19:

Time (s)	Droplet Volume (ml)
0	0.003508751
0.224	0.003157983
0.465	0.002781833
0.680	0.002344756
0.811	0.002025794
0.938	0.001876024
1.082	0.001328848
1.330	0.001023447

Slope = -0.0019 ml/s; R^2 = 0.989

Droplet 20:

Time (s)	Droplet Volume (ml)
0	0.004057811
0.443	0.003218027
0.622	0.002893751
0.733	0.002637841
0.947	0.002028734
1.085	0.001898304
1.322	0.001357024
1.454	0.001139157
1.637	0.001025756

Slope = -0.0020 ml/s; R^2 = 0.990

Summary:

Number of droplets = 20
Mean slope = 2.70 ± 0.55 µl/s

HFA 227ea-EtOH(15% w/w); 37° C, 100% RH

Droplet 1:

Time (s)	Droplet Volume (ml)
0	0.003894045
0.246	0.003257154
0.366	0.002384399
0.594	0.001547191
0.716	0.001252443
0.940	0.000899561

Slope = -0.0034 ml/s; R^2 = 0.961

Droplet 2:

Time (s)	Droplet Volume (ml)
0	0.003621537
0.147	0.003459196
0.332	0.002154874
0.449	0.002234842
0.547	0.001759982
0.679	0.001217195
0.902	0.001135487

Slope = -0.0031 ml/s; R^2 = 0.919

Droplet 3:

Time (s)	Droplet Volume (ml)
0	0.004024843
0.192	0.003518733
0.398	0.002827713
0.560	0.002194261
0.658	0.001837915
0.870	0.001336425
1.038	0.001114378

Slope = -0.0030 ml/s; R^2 = 0.984

Droplet 4:

Time (s)	Droplet Volume (ml)
0	0.003675076
0.242	0.003150478
0.425	0.002473914
0.585	0.002018373
0.740	0.001520544
0.975	0.001028941

Slope = -0.0028 ml/s; $R^2 = 0.993$

Droplet 5:

Time (s)	Droplet Volume (ml)
0	0.004168420
0.209	0.003358197
0.473	0.003127754
0.605	0.002469137
0.769	0.002243215
0.806	0.001837311
0.926	0.001205467
1.120	0.001194372

Slope = -0.0028 ml/s; $R^2 = 0.955$

Droplet 6:

Time (s)	Droplet Volume (ml)
0	0.003760844
0.199	0.003351972
0.421	0.002468242
0.532	0.002105720
0.703	0.001791543
0.811	0.001323774
1.005	0.001139473

Slope = -0.0028 ml/s; $R^2 = 0.979$

Droplet 7:

Time (s)	Droplet Volume (ml)
0	0.003982408
0.201	0.003788127
0.292	0.003169498
0.470	0.002204571
0.632	0.001983715
0.823	0.001305872
0.890	0.001155762
1.146	0.000967018

Slope = -0.0030 ml/s; $R^2 = 0.944$

Droplet 8:

Time (s)	Droplet Volume (ml)
0	0.003720843
0.174	0.002879058
0.333	0.002355480
0.502	0.001675189
0.755	0.001581573
0.956	0.001261837
1.101	0.001113475

Slope = -0.0022 ml/s; $R^2 = 0.898$

Droplet 9:

Time (s)	Droplet Volume (ml)
0	0.003848105
0.175	0.003298271
0.365	0.002480267
0.456	0.002123409
0.687	0.001877319
0.871	0.001405738
1.136	0.001200458

Slope = -0.0024 ml/s; $R^2 = 0.929$

Droplet 10:

Time (s)	Droplet Volume (ml)
0	0.003884381
0.216	0.003705435
0.341	0.003699504
0.442	0.003338172
0.588	0.002879504
0.822	0.001875911
0.994	0.001758621
1.210	0.001182743

Slope = -0.0025 ml/s; $R^2 = 0.951$

Droplet 11:

Time (s)	Droplet Volume (ml)
0	0.003681572
0.181	0.003481274
0.290	0.002718076
0.538	0.002163181
0.729	0.001769931
0.938	0.001249738
1.079	0.001056827

Slope = -0.0025 ml/s; $R^2 = 0.975$

Droplet 12:

Time (s)	Droplet Volume (ml)
0	0.003982087
0.195	0.003362249
0.297	0.003269047
0.447	0.002487331
0.557	0.002216873
0.788	0.001591379
1.009	0.001138735
1.235	0.000983452

Slope = -0.0026 ml/s; $R^2 = 0.965$

Droplet 13:

Time (s)	Droplet Volume (ml)
0	0.004028192
0.158	0.003789054
0.248	0.003622843
0.439	0.002858201
0.693	0.002163941
0.876	0.001787164
1.113	0.001322481
1.248	0.001147359

Slope = -0.0025 ml/s; $R^2 = 0.985$

Droplet 14:

Time (s)	Droplet Volume (ml)
0	0.003879054
0.216	0.003294855
0.320	0.003157735
0.419	0.002789154
0.664	0.002171935
0.863	0.001851834
0.996	0.001669374
1.215	0.001128437

Slope = -0.0022 ml/s; $R^2 = 0.992$

Droplet 15:

Time (s)	Droplet Volume (ml)
0	0.004081375
0.165	0.003952205
0.275	0.003760894
0.449	0.003369348
0.580	0.002784891
0.791	0.002238752
1.048	0.001576913
1.260	0.001278851

Slope = -0.0023 ml/s; $R^2 = 0.977$

Droplet 16:

Time (s)	Droplet Volume (ml)
0	0.003802745
0.209	0.003682241
0.386	0.003222787
0.501	0.002358177
0.724	0.002136844
0.907	0.001751246
1.096	0.001569934
1.367	0.001024844

Slope = -0.0022 ml/s; $R^2 = 0.951$

Droplet 17:

Time (s)	Droplet Volume (ml)
0	0.003459024
0.163	0.003292501
0.294	0.002705438
0.515	0.002114864
0.725	0.001695057
0.951	0.001488702
1.162	0.001136957
1.265	0.001118732

Slope = -0.0019 ml/s; $R^2 = 0.958$

Droplet 18:

Time (s)	Droplet Volume (ml)
0	0.004158236
0.135	0.003890246
0.258	0.003627086
0.447	0.002893402
0.707	0.002157283
0.945	0.001869134
1.196	0.001439925
1.417	0.001206844

Slope = -0.0022 ml/s; $R^2 = 0.970$

Droplet 19:

Time (s)	Droplet Volume (ml)
0	0.003890558
0.134	0.003758106
0.343	0.003369524
0.544	0.003187544
0.801	0.002581739
0.931	0.002554973
1.179	0.002171935
1.343	0.001365781
1.434	0.001328795
1.574	0.001124987

Slope = -0.0018 ml/s; $R^2 = 0.975$

Droplet 20:

Time (s)	Droplet Volume (ml)
0	0.004182056
0.215	0.004067732
0.352	0.003989504
0.579	0.003458197
0.779	0.002780456
0.900	0.002569931
1.022	0.001458382
1.200	0.001439566
1.462	0.001200178

Slope = -0.0024 ml/s; $R^2 = 0.929$

Summary:

Number of droplets = 20
Mean slope = 2.53 ± 0.41 µl/s

HFA 227ea-EtOH(15% w/w)-Sorbitan Trioleate(0.2% w/w); 37° C, < 10% RH

Droplet 1:

Time (s)	Droplet Volume (ml)
0	0.003580247
0.140	0.003382705
0.290	0.002452715
0.498	0.002206844
0.654	0.001835721
0.828	0.001573194
0.921	0.001302594
1.041	0.001128473

Slope = -0.0024 ml/s; R^2 = 0.963

Droplet 2:

Time (s)	Droplet Volume (ml)
0	0.003620875
0.208	0.003125843
0.418	0.002798241
0.531	0.002637415
0.760	0.002127381
0.945	0.001336827
1.120	0.001258874
1.307	0.001002785

Slope = -0.0021 ml/s; R^2 = 0.978

Droplet 3:

Time (s)	Droplet Volume (ml)
0	0.003268754
0.200	0.002859427
0.301	0.002865485
0.557	0.002378254
0.745	0.001857561
0.901	0.001124788
1.111	0.001058732

Slope = -0.0021 ml/s; R^2 = 0.959

Droplet 4:

Time (s)	Droplet Volume (ml)
0	0.003368572
0.167	0.003102847
0.323	0.002487518
0.486	0.002368127
0.709	0.001628045
0.920	0.001537812
1.020	0.001107558
1.234	0.000895715

Slope = -0.0021 ml/s; R^2 = 0.976

Droplet 5:

Time (s)	Droplet Volume (ml)
0	0.003825719
0.120	0.003591272
0.302	0.002980577
0.511	0.002458781
0.683	0.002369985
0.799	0.001805721
0.987	0.001453781
1.326	0.001105765
1.420	0.001052164

Slope = -0.0020 ml/s; R^2 = 0.966

Droplet 6:

Time (s)	Droplet Volume (ml)
0	0.003798054
0.214	0.003452781
0.464	0.002789359
0.594	0.002682545
0.719	0.002284375
0.909	0.001452822
1.140	0.001121271

Slope = -0.0025 ml/s; R^2 = 0.976

Droplet 7:

Time (s)	Droplet Volume (ml)
0	0.003759057
0.203	0.003028437
0.382	0.002580444
0.509	0.002268187
0.621	0.001827391
0.750	0.001322872
1.006	0.001102874

Slope = -0.0028 ml/s; $R^2 = 0.973$

Droplet 8:

Time (s)	Droplet Volume (ml)
0	0.003205784
0.101	0.002549102
0.313	0.002028473
0.473	0.001761274
0.694	0.001225844
0.855	0.001157181

Slope = -0.0023 ml/s; $R^2 = 0.940$

Droplet 9:

Time (s)	Droplet Volume (ml)
0	0.003987511
0.144	0.003650875
0.353	0.002587305
0.473	0.002287951
0.700	0.001643784
0.879	0.001428181
1.043	0.001112467

Slope = -0.0031 ml/s; $R^2 = 0.966$

Droplet 10:

Time (s)	Droplet Volume (ml)
0	0.003848047
0.219	0.003657812
0.319	0.003369187
0.460	0.002458137
0.663	0.002273545
0.753	0.001505708
0.977	0.001258705
1.117	0.001025887

Slope = -0.0028 ml/s; $R^2 = 0.952$

Droplet 11:

Time (s)	Droplet Volume (ml)
0	0.003825774
0.191	0.003328442
0.380	0.002842721
0.527	0.002351908
0.706	0.001937518
0.878	0.001532048
1.067	0.001187541

Slope = -0.0025 ml/s; $R^2 = 0.995$

Droplet 12:

Time (s)	Droplet Volume (ml)
0	0.003750842
0.139	0.003451807
0.250	0.002834789
0.442	0.002251832
0.679	0.001680548
0.887	0.001245765
1.073	0.001024873

Slope = -0.0026 ml/s; $R^2 = 0.972$

Droplet 13:

Time (s)	Droplet Volume (ml)
0	0.004025487
0.200	0.003597810
0.440	0.003125715
0.561	0.002643752
0.675	0.002248774
0.808	0.001657381
1.004	0.001345725
1.112	0.001142187

Slope = -0.0028 ml/s; $R^2 = 0.984$

Droplet 14:

Time (s)	Droplet Volume (ml)
0	0.004284732
0.244	0.003880875
0.428	0.003251804
0.576	0.002584375
0.715	0.002245078
0.988	0.001357427
1.273	0.001124289

Slope = -0.0027 ml/s; $R^2 = 0.971$

Droplet 15:

Time (s)	Droplet Volume (ml)
0	0.003876957
0.184	0.003254875
0.369	0.002784087
0.596	0.002357504
0.810	0.001957105
0.917	0.001657224
1.031	0.001222675
1.167	0.001024878

Slope = -0.0024 ml/s; $R^2 = 0.992$

Droplet 16:

Time (s)	Droplet Volume (ml)
0	0.004157826
0.171	0.003597218
0.278	0.002687287
0.443	0.002564872
0.643	0.002205492
0.874	0.001683708
1.110	0.001254489
1.315	0.001128107

Slope = -0.0022 ml/s; $R^2 = 0.929$

Droplet 17:

Time (s)	Droplet Volume (ml)
0	0.003849375
0.220	0.003321808
0.386	0.002548731
0.477	0.002186375
0.697	0.001987311
0.880	0.001340574
1.140	0.001120567
1.264	0.001124248

Slope = -0.0022 ml/s; $R^2 = 0.934$

Droplet 18:

Time (s)	Droplet Volume (ml)
0	0.003980571
0.098	0.003781279
0.237	0.003558705
0.437	0.002781389
0.7	0.002405768
0.877	0.001558437
1.069	0.001359414
1.209	0.001023748

Slope = -0.0025 ml/s; $R^2 = 0.986$

Droplet 19:

Time (s)	Droplet Volume (ml)
0	0.003505784
0.089	0.003210577
0.253	0.002684057
0.513	0.002210579
0.656	0.001652878
0.841	0.001534877
1.064	0.001205738
1.253	0.000938442

Slope = -0.0020 ml/s; R^2 = 0.967

Droplet 20:

Time (s)	Droplet Volume (ml)
0	0.003405788
0.202	0.003119872
0.340	0.002549872
0.498	0.002218084
0.635	0.001934571
0.961	0.001654872
1.155	0.001364289
1.298	0.001137186

Slope = -0.0017 ml/s; R^2 = 0.959

Summary:

Number of droplets = 20
Mean slope = 2.39 ± 0.35 µl/s

HFA 227ea-EtOH(15% w/w)-Sorbitan Trioleate(0.2% w/w); 37° C, 100% RH

Droplet 1:

Time (s)	Droplet Volume (ml)
0	0.003682741
0.196	0.003250578
0.287	0.002438521
0.448	0.001683748
0.637	0.001205789
0.846	0.001027579

Slope = -0.0034 ml/s; R^2 = 0.927

Droplet 2:

Time (s)	Droplet Volume (ml)
0	0.003458057
0.216	0.003059884
0.330	0.002408721
0.508	0.002039836
0.712	0.001350578
0.976	0.001175466

Slope = -0.0025 ml/s; R^2 = 0.952

Droplet 3:

Time (s)	Droplet Volume (ml)
0	0.003458087
0.160	0.003269983
0.300	0.002820574
0.445	0.002237766
0.640	0.001764184
0.791	0.001422581
0.993	0.001127843

Slope = -0.0026 ml/s; R^2 = 0.981

Droplet 4:

Time (s)	Droplet Volume (ml)
0	0.003982254
0.242	0.003381274
0.398	0.002450872
0.590	0.001852791
0.779	0.001345721
1.014	0.001024783
1.175	0.000983408

Slope = -0.0031 ml/s; $R^2 = 0.964$

Droplet 5:

Time (s)	Droplet Volume (ml)
0	0.003598274
0.106	0.003440874
0.281	0.002893748
0.480	0.002240876
0.687	0.001563782
0.895	0.001359972
1.036	0.001227543
1.075	0.001128738

Slope = -0.0024 ml/s; $R^2 = 0.970$

Droplet 6:

Time (s)	Droplet Volume (ml)
0	0.003562741
0.176	0.003257804
0.401	0.002785315
0.530	0.002269137
0.705	0.001534057
0.875	0.001328774
1.065	0.001154058

Slope = -0.0025 ml/s; $R^2 = 0.966$

Droplet 7:

Time (s)	Droplet Volume (ml)
0	0.003398247
0.165	0.002843708
0.412	0.002429371
0.574	0.001960384
0.727	0.001605741
0.919	0.001352874
1.070	0.001036842

Slope = -0.0022 ml/s; $R^2 = 0.987$

Droplet 8:

Time (s)	Droplet Volume (ml)
0	0.003593784
0.135	0.003120574
0.325	0.002530874
0.490	0.002235409
0.698	0.001789054
0.817	0.001535794
1.064	0.001227846
1.246	0.001139475

Slope = -0.0020 ml/s; $R^2 = 0.956$

Droplet 9:

Time (s)	Droplet Volume (ml)
0	0.003682707
0.186	0.003361725
0.300	0.002890751
0.498	0.002452718
0.746	0.002110573
0.849	0.001988748
0.938	0.001637187
1.086	0.001205741
1.294	0.001135781

Slope = -0.0021 ml/s; $R^2 = 0.980$

Droplet 10:

Time (s)	Droplet Volume (ml)
0	0.003512781
0.154	0.003428871
0.408	0.002450577
0.600	0.002281087
0.711	0.002257491
0.853	0.001650274
1.110	0.001369847
1.248	0.001327078
1.480	0.001023487

Slope = -0.0018 ml/s; $R^2 = 0.953$

Droplet 11:

Time (s)	Droplet Volume (ml)
0	0.003750844
0.161	0.003522842
0.416	0.002468271
0.551	0.002467815
0.743	0.002237811
1.003	0.001532741
1.095	0.001225795
1.203	0.001195271

Slope = -0.0022 ml/s; $R^2 = 0.972$

Droplet 12:

Time (s)	Droplet Volume (ml)
0	0.003512705
0.382	0.002597271
0.557	0.002226874
0.669	0.001937804
0.809	0.001527813
0.987	0.001241087
1.162	0.001033278

Slope = -0.0022 ml/s; $R^2 = 0.989$

Droplet 13:

Time (s)	Droplet Volume (ml)
0	0.003822405
0.212	0.003369475
0.381	0.002780184
0.586	0.002336815
0.843	0.002011574
0.940	0.001781371
1.093	0.001728873
1.260	0.001320578
1.425	0.001123499

Slope = -0.0019 ml/s; $R^2 = 0.975$

Droplet 14:

Time (s)	Droplet Volume (ml)
0	0.003450579
0.163	0.003265187
0.328	0.002672815
0.462	0.002408765
0.609	0.002139172
0.768	0.001652274
0.963	0.001344057
1.159	0.001322579
1.373	0.001124871

Slope = -0.0018 ml/s; $R^2 = 0.947$

Droplet 15:

Time (s)	Droplet Volume (ml)
0	0.003587641
0.240	0.003157284
0.381	0.002851978
0.593	0.002405499
0.777	0.001980574
0.980	0.001508705
1.222	0.001320278
1.380	0.001122984

Slope = -0.0019 ml/s; $R^2 = 0.985$

Droplet 16:

Time (s)	Droplet Volume (ml)
0	0.003428127
0.205	0.003220571
0.330	0.002542087
0.505	0.001591374
0.747	0.001236597
0.969	0.001024872

Slope = -0.0019 ml/s; $R^2 = 0.985$

Droplet 17:

Time (s)	Droplet Volume (ml)
0	0.003581375
0.409	0.002450574
0.571	0.001938732
0.682	0.001425874
0.904	0.001124687
1.060	0.001102687

Slope = -0.0025 ml/s; $R^2 = 0.952$

Droplet 18:

Time (s)	Droplet Volume (ml)
0	0.003498271
0.144	0.003203891
0.349	0.002450879
0.559	0.002234199
0.707	0.001637481
0.846	0.001311087
1.061	0.001124914

Slope = -0.0024 ml/s; $R^2 = 0.975$

Droplet 19:

Time (s)	Droplet Volume (ml)
0	0.003798524
0.198	0.003528105
0.375	0.002794327
0.550	0.002405183
0.695	0.001934681
0.782	0.001537844
0.923	0.001322549
1.176	0.001124638

Slope = -0.0025 ml/s; $R^2 = 0.964$

Droplet 20:

Time (s)	Droplet Volume (ml)
0	0.003762157
0.159	0.003421876
0.409	0.002408421
0.571	0.002231698
0.817	0.001451873
1.019	0.001362842
1.262	0.001124938
1.419	0.000899154

Slope = -0.0020 ml/s; $R^2 = 0.940$

Summary:

Number of droplets = 20
Mean slope = 2.34 ± 0.42 µl/s

Appendix B

Bench Test Data

37° C, < 10% RH; 15 cm tubing

	MMAD (μm)		GSD		Spacer Deposition (%)	
run	Airomir	Ventolin	Airomir	Ventolin	Airomir	Ventolin
1	2.03	2.06	1.22	1.47	40.82	55.55
2	2.06	1.95	1.48	1.47	30.37	63.85
3	1.82	2.15	1.44	1.54	41.61	60.19
4	1.92	1.98	1.46	1.49	40.83	63.31
5	1.84	1.92	1.44	1.48	39.34	72.73
Mean	1.93	2.01	1.41	1.49	38.59	63.13
Std. Dev.	0.11	0.09	0.11	0.03	4.67	6.30

37° C, 100% RH; 15 cm tubing

	MMAD (μm)		GSD		Spacer Deposition (%)	
run	Airomir	Ventolin	Airomir	Ventolin	Airomir	Ventolin
1	3.70	3.92	1.23	1.26	51.49	71.48
2	3.79	3.83	1.24	1.27	54.68	72.62
3	3.76	3.88	1.23	1.24	50.44	65.52
4	3.67	3.83	1.23	1.26	52.50	73.85
5	3.70	3.81	1.21	1.23	51.91	75.01
Mean	3.72	3.85	1.23	1.25	52.20	71.70
Std. Dev.	0.05	0.05	0.01	0.02	1.58	3.70

37° C, < 10% RH; 45 cm tubing

	MMAD (μm)		GSD		Spacer Deposition (%)	
run	Airomir	Ventolin	Airomir	Ventolin	Airomir	Ventolin
1	2.00	2.04	1.20	1.54	42.06	73.42
2	1.87	1.75	1.45	1.51	35.88	66.39
3	2.03	1.98	1.22	1.48	42.81	52.66
Mean	1.97	1.92	1.29	1.51	40.25	64.16
Std. Dev.	0.09	0.15	0.14	0.03	3.80	10.56

37° C, 100% RH; 45 cm tubing

	MMAD (μm)		GSD		Spacer Deposition (%)	
run	Airomir	Ventolin	Airomir	Ventolin	Airomir	Ventolin
1	3.56	3.70	1.39	1.31	43.80	75.00
2	3.62	3.61	1.32	1.46	48.71	68.67
3	3.39	3.50	1.37	1.36	51.12	75.20
Mean	3.52	3.60	1.36	1.38	47.88	72.96
Std. Dev.	0.12	0.10	0.04	0.08	3.73	3.71

Appendix C

MATLAB Script to Calculate MMAD and GSD from Cascade Impactor Data

```
% MMAD and GSD calculator
% Fits a log-normal distribution function to
% percentage mass distibution data from an
% Andersen cascade impactor.

% Andrew Martin, Nov. 2003

sizes = [0.55, 0.9, 1.6, 2.7, 4, 5.25, 7.4];    %Midpoints between Andersen impactor plates
intervals = [0.3, 0.4, 1, 1.2, 1.4, 1.1, 3.2];  %Spacing between plates
rawdata = [1.00, 6.90, 63.05, 27.65, 1.02, 0.20, 0.18];  %Non-Cum percentage distribution, plate
↪ 7 downto 1

data = rawdata./(100*intervals);
x0 = [2.0,2.0];    %inital guess at MMAD, GSD
MMDGSDfit = inline('exp(-(log(sizes)-
↪log(x(1))).^2./(2*(log(x(2))).^2))./(sizes.*sqrt(2*pi).*log(x(2)))','x','sizes');
[x,resid] = lsqcurvefit(MMDGSDfit,x0,sizes,data)
```

Appendix D

MATLAB Scripts to Determine Wet-Bulb Temperatures of Spherical HFA Droplets

```
%Droplet Lifetimes for HFA 134a between -70C and 20C
%Andrew Martin
%May 14, 2002 (Updated Feb 5, 2004)

%Set ambient temperature, pressure
d = 0.00002
Tinf = 37+273.15;
Pinf = 101320;
Ts = -62+273.15;%     <---- change this value to find Ts giving f(Ts)=0

%Calculate droplet properties
k134s = 10^(-3)*(-13.44168+0.0921486*Ts);
liqdens_134s = -3.1962*Ts + 2160;
D = -5.725646*10^-6 + 5.265307*10^-8*Tinf;
Ds = -5.725646*10^-6 + 5.265307*10^-8*Ts;
Cp134 = 1000*(-0.06682556+0.003577778*Tinf);
Cp134s = 1000*(-0.06682556+0.003577778*Ts)
R134 = 81.56;
u134s = -9.4602778*10^-7 + 4.389*10^-8*Ts;
Ls = 1000*(388.3988-0.7025714*Ts);
ps = 6.021795*10^9*exp(-2714.4749/Ts);
M134 = 0.102;

%Calculate air properties
kair = 0.0017 + 0.000082*Tinf;
kairs = 0.0017 + 0.000082*Ts;
uairs = 2.83*10^-6 + 5.21*10^-8*Ts;
Rair = 287;
Mair = 0.02897;

%Mass fraction for droplet
Ys = (ps*M134)/(ps*M134+(Pinf-ps)*Mair);
Yinf = 0; %no vapor in ambient air

%Lewis Numbers
Le_inf = (kair*Rair*Tinf)/(Pinf*Cp134*D);
dens_134s = ps/(R134*Ts);
dens_airs = (Pinf-ps)/(Rair*Ts);
dens_s = dens_134s + dens_airs;
X134s = (dens_134s/M134)/(dens_134s/M134 + dens_airs/Mair);
Xairs = (dens_airs/Mair)/(dens_134s/M134 + dens_airs/Mair); %mole fractions
PHI134 = 8^(-1/2)*(1+M134/Mair)^(-1/2)*(1+(u134s/uairs)^(1/2)*(Mair/M134)^(1/4))^2;
PHIair = 8^(-1/2)*(1+Mair/M134)^(-1/2)*(1+(uairs/u134s)^(1/2)*(M134/Mair)^(1/4))^2;
ks = (X134s*k134s)/(X134s+Xairs*PHI134) + (Xairs*kairs)/(Xairs+X134s*PHIair);
Le_s = ks/(dens_s*Cp134s*Ds);
Le = (Le_s*Le_inf)^(1/2);

%Finlay, Eq. (4.108)
f = log(Cp134s*(Tinf-Ts)/Ls + 1) + log((1-Ys)/(1-Yinf))/Le

%Evaporation rate
B = log(Cp134s*(Tinf-Ts)/Ls + 1)
dmdt = -2*pi*d*ks*B/Cp134s
dddt_cm = -4*ks*B/(liqdens_134s*d*Cp134s)*100
tL = liqdens_134s*d*d*Cp134s/(8*ks*B)
```

```
%Droplet Lifetimes for HFA 227ea
%Andrew Martin
%Feb 10, 2003

%Set ambient temperature, pressure
d = 0.00002
Tinf = 37 + 273.15;
Pinf = 101320;
Ts = -51 + 273.15;% <---- change this value to find Ts giving f(Ts)=0

%Calculate droplet properties (for -40C to 40C from Dupont Data)
liqdens_227s = -3.7686*Ts + 2509.014647;
k227s = 10^(-3)*(-8.257712+0.0702353*Ts);
D = -4.27808*10^-6 + 3.49637*10^-8*Tinf;
Ds = -4.27808*10^-6 + 3.49637*10^-8*Ts;
Cp227 = 1000*(-0.1518642574+0.003576421569*Tinf);
Cp227s = 1000*(-0.1518642574+0.003576421569*Ts);
R227 = 44.5915; %average from -40C to 40C every 5C
u227s = -3.79656*10^-7 + 3.96667*10^-8*Ts;
Ls = 1000*(270.1474871-0.518227*Ts);
ps = 0.591928033*(1.047767)^Ts; %data from -40C to 0
M227 = 0.17003;

%Calculate air properties
kair = 0.0017 + 0.000082*Tinf;
kairs = 0.0017 + 0.000082*Ts;
uairs = 2.83*10^-6 + 5.21*10^-8*Ts;
Rair = 287;
Mair = 0.02897;

%Mass fraction for droplet
Ys = (ps*M227)/(ps*M227+(Pinf-ps)*Mair);
Yinf = 0.0;                    %no vapor in ambient air

%Lewis Numbers
Le_inf = (kair*Rair*Tinf)/(Pinf*Cp227*D);
dens_227s = ps/(R227*Ts);
dens_airs = (Pinf-ps)/(Rair*Ts);
dens_s = dens_227s + dens_airs;
X227s = (dens_227s/M227)/(dens_227s/M227 + dens_airs/Mair);
Xairs = (dens_airs/Mair)/(dens_227s/M227 + dens_airs/Mair); %mole fractions
PHI227 = 8^(-1/2)*(1+M227/Mair)^(-1/2)*(1+(u227s/uairs)^(1/2)*(Mair/M227)^(1/4))^2;
PHIair = 8^(-1/2)*(1+Mair/M227)^(-1/2)*(1+(uairs/u227s)^(1/2)*(M227/Mair)^(1/4))^2;
ks = (X227s*k227s)/(X227s+Xairs*PHI227) + (Xairs*kairs)/(Xairs+X227s*PHIair);
Le_s = ks/(dens_s*Cp227s*Ds);
Le = (Le_s*Le_inf)^(1/2);

%Finlay, Eq. (4.108)
f = log(Cp227s*(Tinf-Ts)/Ls + 1) + log((1-Ys)/(1-Yinf))/Le

%Evaporation rate
B = log(Cp227s*(Tinf-Ts)/Ls + 1)
dmdt = -2*pi*d*ks*B/Cp227s
dddt_cm = -4*ks*B/(liqdens_227s*d*Cp227s)*100
dvdt_cm = dmdt/liqdens_227s * 100^3
tL = liqdens_227s*d*d*Cp227s/(8*ks*B)
```